BIOACTIVE GLASS COATED SILICONE FOR PERCUTANEOUS DEVICES WITH IMPROVED TISSUE INTERACTION

By

JAMES SCOTT MAROTTA

DISSERTATION PRESENTED TO THE GRADUATE SCHOOL
OF THE UNIVERSITY OF FLORIDA IN PARTIAL FULFILLMENT
OF THE REQUIREMENTS FOR THE DEGREE OF
DOCTOR OF PHILOSOPHY

UNIVERSITY OF FLORIDA

1997

This dissertation is dedicated to
my family without whose love and support
could not have come this far.

ACKNOWLEDGMENTS

I would like to express my gratitude to my advisor and committee chairman, Dr. Christopher D. Batich, for his encouragement, guidance and patience. Special appreciation is also felt for Dr. Eugene P. Goldberg for his confidence, support and guidance. Thanks are also extended to the members of my supervisory committee for their advice and teaching, Dr. Anthony B. Brennan, Dr. Larry L. Hench and Dr. Karen A. Holbrook.

Appreciation is also extended to my colleagues for their invaluable assistance and encouragement during my graduate studies. They are Drew Amery, Travis Arcia, Jesse Arnold, Gwen Clark, Shannon Eggers, Bob Hadba, Penelope Kao, James Kirk, Guy LaTorre, Paul Martin, Tom Miller, Rodrigo Orefice, Lei Wei, Dr. John West, Dr. Chris Widenhouse, John Wironen, Stacey Zambo, and Mike Zamora. Special thanks are felt for Jackie Huisey for keeping everything on the 3rd floor from getting completely out of hand. Thanks are also given to the Adair, Brennan, Goldberg, and Hench groups and U.S. Biomaterials for all of the material and equipment they let me borrow (sometimes with permission).

TABLE OF CONTENTS

LIST OF TABLES

LIST OF FIGURES

KEY TO SYMBOLS

	symbol
Bioactivity Index	I_B
Calcium-Phosphate Layer	CaP
Centimeter	cm
Circular Halo Samples	C13
Cubic Centimeter (cm^3)	cc
Degree Centigrade	°C
Fourier Transform Infrared Spectroscopy	FTIR
Gram	g
Gel Permeation Chromatograph	GPC
Hydroxyapatite, $Ca_5(PO_4)_3OH$	HAP
Hydroxycarbonate Apatite	HCA
hydrochloric acid	HCl
Inductively Coupled Plasma Spectroscopy	ICP
Liter	L
Micrometer (10^{-6} meter)	µm
Milliliter (10^{-3} Liter)	mL
Millimeter (10^{-3} meter)	mm
Peritoneal Dialysis	PD
Poly(ethylene terephthalate)	PET
Poly-ether sulfone	PESF
Photomultiplier Tube Voltages	PMT
Pressure (1 Torr = 1 mm mercury)	Torr
Rectangular Halo samples	R13
Simulated Body Fluid	SBF
1.5 times Simulated Body Fluid	1.5SBF
Scanning Electron Microscopy	SEM
Surface Area to Volume Ratio	SA/V
Tetra(ethoxysilane)	TEOS
Thousand Electron Volts	keV
Tris(hyroxymethyl) aminomethane	THAM
Weight to Volume Ratio	W/V
X-ray Photoelectron Spectroscopy	XPS

Abstract of Dissertation Presented to the Graduate School of the University of Florida in Partial Fulfillment of the Requirements for the Degree of Doctor of Philosophy

BIOACTIVE GLASS COATED SILICONE FOR PERCUTANEOUS DEVICES WITH IMPROVED TISSUE INTERACTION

By

JAMES SCOTT MAROTTA

August, 1997

Chairperson: Dr. Christopher D. Batich
Major Department: Materials Science and Engineering

The discovery of bioactive glasses, in the early 1970s, has produced a material that develops a strong adherent bond with soft tissue. Many medical applications currently use silicone as an implant material, but are hindered by the formation of fibrous scar tissue surrounding the device. This fibrous scar tissue can lead to pain, infection, and/or extrusion of these devices. Bioactive ceramic materials are inherently brittle and can not be used in applications where a flexible material is needed. Therefore, the coating of existing flexible silicone medical devices, like catheters, with a bioactive glass material would give the advantages of both

The research presented here is of methods used to coat silicone with a bioactive glass powder (Bioglass®) and the *in vitro* testing of those coatings. The bioactivity of these coatings was measured using scanning electron microscopy, inductively coupled plasma spectroscopy, and Fourier transform infrared spectroscopy. It was observed that hydroxyapatite, a bonelike apatite, was formed *in vitro* on both the bioactive glass particles and the silicone surface between these particles. From these results a new theory was developed that related the distance between particles on a surface with the formation of an apatite layer. A critical distance between particles for the formation of an apatite layer on the substrate exists. This critical distance is a function of both the particle size and composition. In addition, a method to coat silicone catheters with bioactive glass powder is also discussed.

This coated catheter could ultimately be used for improved percutaneous access in peritoneal dialysis. The one barrier to greater peritoneal dialysis use and the reason many patients switch from peritoneal to hemodialysis is recurrent exit-site infections and subsequent peritonitis. These infections are caused by the lack of a tight seal and downgrowth of epidermal tissue around the catheter at the catheter-skin interface.

CHAPTER 1
INTRODUCTION

The design of a percutaneous, through the skin, access device is one of the most challenging problems that faces the medical community today. The epidermis by its very nature is an effective barrier to access and will try to extrude or wall-off any foreign objects that penetrate it. Current medical devices that provide long-term percutaneous access for peritoneal dialysis, consist of catheters with fabric cuffs that are placed subcutaneous to anchor the device with scar tissue. The subcutaneous scar tissue forms early in the healing process and provides an anchor for the device at the exit-site. During a longer term, the epithelial tissue tunnels down around the catheter until it reaches the cuff site. This downgrowth provides access to bacteria and other pathogens that cause infection.

Despite the use of cuffs to limit the sinus tract length, no catheter in use today can provide "significant prevention of exit-site/tunnel infections" (Luzi, p.335) in peritoneal dialysis. The reduction of exit-site infections is considered an integral part of peritoneal dialysis.

advancement (Twa94, Fel95, Ash94 and USR96c). The healing pattern that forms around these devices, epithelial downgrowth, lacks soft tissue adhesion and the epithelium is observed to stop when it contacts the healthy collagenous tissue at the Dacron cuff(Twa92 and Win74).

Bioactive glasses have shown excellent soft tissue healing and adhesion (Wil90 and Hen93a). This adhesion is attributed to the direct bonding of collagen fibers to the glass surface during hydroxyapatite formation (Wil81, Ito87, and Hen84). This apatite layer formed on the bioactive glass surface is the same phase as biological or bone-like apatite formed in tissue(Hen93a). While this study has mainly used Bioglass® powders, the applications are general and should work for most any bioactive glass or glass-ceramic powder.

HYPOTHESIS: Coating silicone devices with a bioactive glass will allow for improved soft tissue adhesion without formation of an intervening fibrous capsule, stop or reduce the epithelial downgrowth, and create a better seal that prevents bacterial access and infection.

CHAPTER 2
BACKGROUND AND REVIEW OF LITERATURE

2.1 Percutaneous Devices

One of the most common percutaneous devices used today is the peritoneal dialysis (PD) catheter. This long-term indwelling catheter provides access to the peritoneal cavity for the exchange of dialysis fluids that clear the cavity of waste products (see Figure 2-1). The basic design and complications that exist with this device are shared with most other percutaneous-access devices and therefore this background will center on the design and complications associated with these types of catheters.

2.1.1 Basic Design

A peritoneal dialysis catheter consists of a tube, usually made of silicone, that provides access through the skin to the peritoneal cavity. The intraperitoneal end of the catheter has multiple perforations and can be either straight, curled or disk shaped. The intramural portion of the catheter can also be either straight or coiled (Monc94).

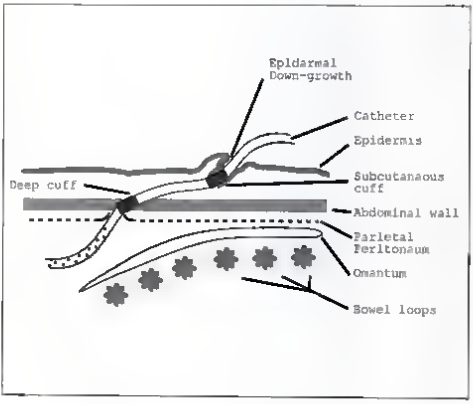

Figura 2-1 Cross section of a double cuff peritoneal dialysis catheter, showing preferred location of cuffs (Adapted from Ash94)

The catheter may have either one or two Dacron® (registered trademark Dupont, Wilmington, DE) fabric cuffs attached. The purpose of the cuffs is to stabilize the catheter by fibrous tissue ingrowth(Taw94). The passageway formed by the catheter through the abdominal wall is defined as the tunnel. The number and position of the cuffs used determines what type of tunnel is formed (see Figure 2-2).

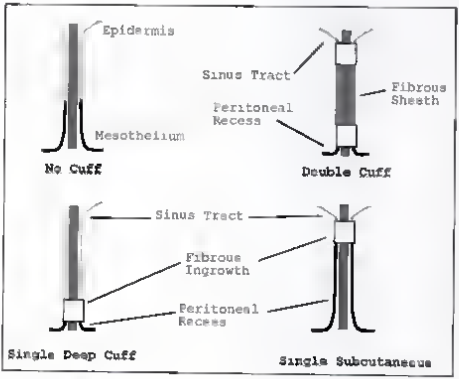

Figure 2-2 Tissue tunnel structures form as a result of cuff position. (Adapted from Taw94)

A single deep cuff would produce a long sinus tract of tissue and be prone to exit-site infections. A single subcutaneous cuff would produce a long Peritoneal Recess and be prone to pseudohernias. The use of a catheter with two cuffs limits both of these and forms a tunnel with a short sinus tract, short peritoneal recess, and a sheath of fibrous scar tissue covering the catheter segment between the two cuffs(Tws94). Authors have suggested that this double-cuff design is better at preventing infection, but thus far there have been no clinical studies that have resolved this issue (Luz91). Other authors have concluded that the tissue ingrowth of the catheter's cuff is the reason for their failure of the devices (Von84 and Paq96a). Despite these ambiguities the majority of catheters used today consist of a double cuff design.

2.1.2 Wound-healing Around Percutaneous Devices

During healing of a properly placed catheter, a blood clot first forms and fills the Dacron® cuff. This clot is slowly replaced by macrophages, fibroblasts and new capillaries. Macrophages surround the individual cuff fibers and collagen forms around them. After 6 weeks healing, a strong fibrous tissue is formed throughout the cuff (Tws94). Healing of the sinus tract begins with epidermal cells spreading beneath the exit scab. These

ri continue to spread until they encounter epithelial cells from the opposite side or dense healthy collagen fibers (Win74, Hal75, and Kan80). This epithelial downgrowth is believed to be stopped by the dense fibrous tissue present in the Dacron® cuff(Twa88 and Aah90) The theory that dense collagen fibers inhibit epithelial downgrowth was first described by Winter (Win74), and has led to development of percutaneous devices that encouraged large amounts of fibrous ingrowth (Kan80, Dal84, and Jan94). Other researchers have made devices of silicone that are coated with a dense fibrous collagen (Suh94 and Oka95). Implanted percutaneously in rabbits these collagen immobilized implants show reduced bacterial infection at the exit-site (Oka95).

2.1.3 Peritonitis

Many PD infections occurring early in the history of their usage, were caused either by poor catheter placement or lack of aseptic technique by patients during fluid changes. By positioning the catheter's tunnel in a downward direction at the exit site; sweat, dirt and pus can drain down, ont and away from the exit-site. Training the patient in proper aseptic technique and the use of improved "quick-connect" ports has reduced the number of patient-related infections. These improvements have been associated with a

reduction in the infection rate from 1 per patient month to 0.1 pat patient year(Gok94 and Gup96). But, despite these improvements exit-site and tunnel infections are still a serious complication and are the major cause of catheter removal and mortality(Kea94, Vas94 and Paq96b). The number of patients switching from PD to hemodialysis parallels the catheter-loss rate (Suh95). Studies indicate that 45% of children on PD switch to hemodialysis because of excessive and recurrent catheter-related infections (Maj97).

Catheter removal and treatment

Exit-site/tunnel infections are a serious complication to peritoneal dialysis and most authors conclude that they infrequently resolve without catheter removal (Gup96 and Maj97). Recent studies have suggested that only the subcutaneous cuff need be removed (Che95 and Suh95). In the later study, the authors concluded that removal of the catheter's cuff in patients with persistent exit-site/tunnel infections can significantly reduce the rate of catheter loss associated with those infections (Suh95). These results suggested that the cuff, once infected, may become a depot for recurrent infections. Despite these complications, the benefits of cost, greater freedom and quality of life have resulted in a continued increase in the use of PD, at twice the rate of hemodialysis (Gok94).

2.1.4 Growth of Peritoneal Dialysis

The growth of peritoneal dialysis has been dramatic over the 27 years of its existence. The increase has been from less than 5,000 patients worldwide in 1979 to more than 85,000 in 1995 (Nia95 and USR96a). The reasons for this rapid growth are the decrease in complication rates, the improved quality of life and increased freedom that PD offers a patient. The usage of PD varies widely for different countries and may be a factor of the reduced cost associated with PD. Third world countries have a very high percentage of their dialysis patients on PD, some have higher than 75% on PD (USR96a). One study concluded that home-based PD had a much lower cost associated with it compared to hospital-based hemodialysis (Coy96). The study found that hemodialysis had much higher physicians' fees, treatment cost and overhead costs than PD. The total annual costs, in Canadian dollars, of a typical PD treatment was $47,569 compared to a typical hemodialysis treatment cost of $76,023 (Coy96 and USR96b).

Current research

It has been concluded that the problem of infection remains the major barrier to greater PD usage (Luz91, Gok93, Ash94 and Twa94). This need for improved percutaneous access has encouraged research efforts into both coatings

and design changes Percutaneous implants have been tested that are anchored to either the cranium or tibia of animals (Jan90a and Jan90b) The authors concluded that stabilization of a percutaneous implant was a requirement for a successful percutaneous passage Realizing that there are many percutaneous access situations which can not be anchored to bone, this group tested an access device consisting of a 3 cm by 4 cm sintered titanium fiber mesh implanted subcutaneously and then attached to a Teflon percutaneous component (Jan91 and Jan94). Fibrous tissue ingrowth of the titanium mesh was intended to stabilize the implant. Early results with this implant showed that failure by tearing of the fiber mesh occurred in 30% of the animals at 4 months (Jan91) In addition, epidermal downgrowth occurred along the Teflon component Reinforcement of the titanium mesh at the attachment site reduced mesh failures to 10%, but significant epidermal downgrowth with sinus formation still occurred (Jan94).

The use of metal antimicrobial coatings, such as silver, has also been the subject of research efforts. Bard Access Systems (Salt Lake City, UT) currently manufactures an antimicrobial cuff (VitaCuff®) that is made of silver impregnated collagen The porous collagen absorbs while implanted allowing for tissue ingrowth Silver ions

leaching from the cnff provide antimicrobial activity. Clinical stndy of the effectivenass of VitaCuff® nsed with central venous catheters concluded that cathater-related sepsis did not differ in frequancy between these catheters and the control cathetars (Sma95) The antimicrobial activity occnrs dnring the first 4 to 6 weaks(Bar94). The Spire Corporation (Bedford, MA) has recently patented ion-beam deposition of silver as an antimicrobial coating on catheter surfaces This coating is limited to only a few microns of the onter catheter surface and is currently being studied *in vivo* and in preliminary clinical trials(Sio94). The nse of antibiotic coatings are a snggested supplement to patient aseptic cleaning of the cathater site dnring early healing(Sha93 and Orr93) It is nnclear how effective these antibiotic coated devices will be over the long-term.

One experimental device that has sncceasfnlly reduced the amonnt of epidermal downgrowth in percutaneous implantation is made of sintered hydroxyapatite (HAP). HAP, $Ca_5(PO_4)_3OH$, a calcium phosphate minaral, is a major componant of bone This material has been usad in madicine and dentistry for more than 20 years (Hen91). A comparative study batwaen percutaneons devicas made of HAP and silicona showad that the silicona devices had epidermal downgrowth that reached the bottom of the implant and a high rate of

infection and extrusion of the implant after only 3 months. HAP devices revealed limited epidermal downgrowth (≥ 1 mm) at 7 months and a mild infection at 17 months (Ako87). In an additional animal PD study, dogs survived for 432 days on PD using an HAP percutaneous-access device/catheter without exit-site infection (Yos91). The authors of this later study observed a "tight and sterile seal between the HAP device and skin tissue" (Yos91, p. 297 and Yos92, p. 219). The suggestion that bioactive ceramics, like HAP, could be used to provide improved PD access has been made in recent review articles (Ren91 and Gok93).

2.2 Bioactive Ceramics

Bioceramics may be characterized in one of three groups: nearly inert, surface-active, and resorbable (Hen82). Inert bioceramics undergo almost no chemical change during implantation. Tissue response to these materials, much like that observed to silicone, is the formation of a fibrous scar capsule around the implant. Examples of inert bioceramics are alumina and carbon. Resorbable bioceramics, like calcium sulfate, degrade gradually while implanted in the body and are slowly replaced by the surrounding tissue. The formation of a bond

batwaan host tissua and tha matariai surfaca ia ona of tha intandad functions of a surface-activa biocaramic. Thia bond is tha result of a spacific biological rasponaa at tha tiasua-implant intarfaca.

2.2.1 Bioactive Glasses

In 1969 it waa discovered by Hanch and colleagues that bona could bond to certain giass compositions (Hen71). This group of bioactiva glasses, called Bioglass®, ara composed of SiO_2, Na_2O, CaO and P_2O_5. Latar work by Wilson and Hench indicatad that tha most reactiva giass compositions, 42 to 52 mol% SiO_2, could davalop an adharant bond to soft tissue (Wil90). Bioglass® 45s5 is tha most studied composition and contains 45% SiO_2, 24.5% Na_2O, 24.5% CaO and 6% P_2O_5, all in weight% (Bioglass® is a ragistarad trademark of tha University of Florida).

Tha baaia of the bonding of bioactiva glassas to tissua is a chemical reaction at tha giass surface that raaults in tha formation of an hydroxycarbonata apatita (HCA) layar in body fluids. Thraa reactions occur on the glaas surface when exposed to an aquaous solution: laaching, dissolution, and pracipitation. These raactions hava been extansivaly atudied by rasaarchars and ara summarizad by 5 raactions stagas shown in Tabla 2-1 (Hen93a). During tha leaching raaction (staga 1), an ion exchange with H^+ or H_3O^+, in

solution, causes the release of alkali or alkaline earth elements from the glass surface into the surrounding fluid

Table 2-1 Reaction stages of bioactive glass (Hen93a).

Stage	
1	Rapid ion exchange of Na^+, Ca^{2+}, or K^+ with H^+ or H_3O^+ $Si\text{-}O\text{-}Na^+ + H^+ \rightarrow Si\text{-}OH^+ + Na^+$
2	Breaking of Si-O-Si bonds resulting in the loss of soluble silica in the form of $Si(OH)_4$ and the formation of Si-OH at the glass surface: $Si\text{-}O\text{-}Si + H_2O \rightarrow Si\text{-}OH + HO\text{-}Si$
3	Condensation and repolymerization of silica-rich layer on the surface $O\text{-}Si\text{-}OH + HO\text{-}Si\text{-}O \rightarrow O\text{-}Si\ O\text{-}Si\text{-}O + H_2O$
4	Migration of Ca^{2+} and PO_4^{3-} groups through the silica-rich layer to the surface forming a $CaO\text{-}P_2O_5$ rich film, followed by growth of the amorphous $CaO\text{-}P_2O_5$-rich film by incorporation of soluble calcium and phosphate from solution
5	Crystallization of the amorphous $CaO\text{-}P_2O_5$ film by incorporation of OH^- or CO_3^{2-} from solution to form hydroxyl or carbonate apatite layer.

These network-modifying ions are not part of the glass network and are rapidly released causing an increase in the interfacial pH. Stage 2, involves the breaking of the silica glass network bonds (-Si-O-Si-O-Si-) causing the dissolution of silica into solution in the form of silicic acid ($Si(OH)_4$). The rate of this dissolution is a factor of

the number of bridging oxygen bonds in the glass network and is extremely slow for compositions of >60% SiO_2. Stages 1 and 2 are reactions that occur simultaneously at the glass-water interface (Ada84). The resulting silanols on the surface of the glass react by polycondensation to form a silica-rich gel layer (Stage 3). In Stage 4, a precipitation reaction takes place, calcium and phosphate ions migrate to the surface of the glass and along with those in solution form an amorphous calcium-phosphate layer (CaP) on and within the silica-rich gel. This CaP layer crystallizes to hydroxycarbonate apatite (HCA) by incorporating CO_3^{2-} anions and water from solution.

The reactions that occur during these 5 stages can be monitored by using Fourier transform infrared reflection (FTIR) spectroscopy. FTIR analysis reveals the types and amount of molecular bonds that are present at the glass surface. Several review papers have summarized the use of FTIR analysis to monitor these changes on bioactive glass surfaces (Rim89, Cla90, Kok90b and Hen91). Due to the scattering induced by the uneven texture of the HCA surface layer formed, diffuse infrared reflectance, rather than specular reflectance, is used to analyze these glasses (Hsn93a). An example of FTIR analysis of Bioglass® disks reacted in Tris buffer for 0, 1, and 2 hours at 37°C are

shown in Figure 2-3 The amorphous CaP and silica-gel layer are seen at 1 hour Crystalline HCA is seen at 2 hours

The molecular bond vibrations that are of interest in the analysis of bioactive glasses are Si-O-Si stretching and bending vibrations, indicative of a silica-gel layer; and P-O stretching and bending vibrations, indicative of a calcium phosphate layer Indicative of the transformation of HAP to an HCA layer on the surface, these P-O bending vibrations split from 1 amorphous bond near 580 cm^{-1} to 3 crystalline bonds at 610, 574 and 566 cm^{-1} The infrared frequencies and band assignments of these molecular bonds have been established for bioactive glass reactions and are shown in Table 2-2 (And90). This table depicts the surface changes on 45s5 Bioglass® with reaction time in Tris buffer

This HCA layer formed on bioactive glasses is the same phase as biological apatite formed in tissue and is necessary for the formation of a bond with tissue to occur (Hen93a). The rate of its formation has been used to evaluate the Bioactivity Index (I_b) of various glasses (Hsn93a) During the precipitation reaction collagen fibrils, present near the glass surface, are incorporated within the HCA layer and result in a bonding of tissue to the glass surface(Zho94)

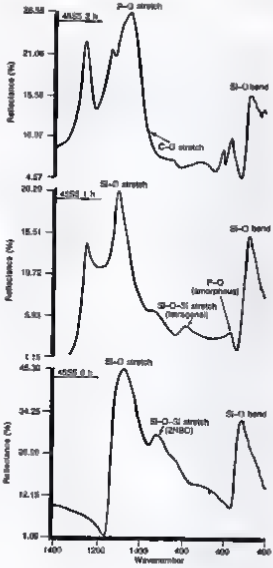

Figure 2-3 FTIR spectra of a 45s5 Bioglass® disk after 0, 1 and 2 hours in Tris buffer at 37°C (Hen91).

Infrared frequencies (cm^{-1}) and band assignments for 45s5 bioactive glass (A[illegible])

Reaction Time (minutes)									Band Assignment
0	2	10	30	45	60	120	180	360	
1098	1095	1096	1095	1095	1097	1088	1099	1100	Si-O str
						1050	1060	1078	P O str
	1018	1010							Si-O str (1NBO)
838	920	898	880						Si-O str (2NBO)
			960	950	850				C-O str
			818	783	777	778			Si-O-Si tetra
						610	610	610	P-O bend cryst
		598	586	577	570	566			P O bend amph
						574	574	574	P-O bend cryst
						566	566	566	P-O bend cryst
510	508	470	468	480	473	455	450	420	Si-O-Si bend

2.2.2 Soft Tissue Interactions

Some of the evidence of soft tissue bonding to Bioglass® came from a comparative study of materials used in facial augmentation (Wil88). In this study of adult dogs, Bioglass® was shown to bond macroscopically to soft tissue (overlying nasal, maxilla and chin facial tissues), it was so firmly bonded that the tissue had to "be forcibly stripped" (Wil88, p 166) from the samples to remove it. Silicone samples at these same sites eroded the underlying bone and developed a thin, non-adherent fibrous capsule. Other studies have confirmed this direct soft tissue adhesion (in tissue of rat dorsal subcutaneous, rat intramuscular and canine gingiva) to Bioglass®, without the formation of a fibrous capsule (Wil81, Ito87, and Hen84). In all of these studies, evidence of direct attachment of collagen fibrils to the glass surface was noted.

Bioglass® has been used to manufacture commercially available middle ear prosthetic devices for the treatment of hearing loss. These devices provide a connection between the soft connective tissues of the tympanic membrane and the oval window, replacing the ossicles. A major mode of failure of implants made of other materials is extrusion through the tympanic membrane (Wil90). Devices made of Bioglass® bond to the soft tissue of the tympanic membrane,

[illegible]ating that mode of failure, and have been in use [illegible]ically for 12 years (Wil93b). Another clinical success of Bioglass® bonding to soft tissue is with endosseous ridge maintenance implants. These conical devices are placed in the alveolar ridge after tooth extraction to maintain ridge morphology (Wil90). These implants have also been clinically used for several years and have been shown to bond to the soft connective tissue of gingiva by collagen fibers bonding within the silica-gel/HCA layer on the surface of the implant (Wil93a and Wil93b)

2.2.3 Bioactive Ceramic Coatings

Some of the earliest coating applications of Bioglass® were on metal femoral implants. These coatings were either dip coated from molten glass, flame-spray coated or fired onto the metal with an enamel frit(Duc85 and Han93b). These techniques use very high temperatures to melt the glass onto the substrate, produce brittle coatings and are not suitable to coat polymer substrates.

The precipitation of a bonelike apatite layer on a polymer surface is not a trivial reaction. Polymers can have highly hydrophobic surfaces that inherently repel the hydrophilic, concentrated calcium phosphate solutions that are used in the precipitation of HA on a surface. Experience in our lab has shown that these solutions will not spread

[illegible] over the silicone surface, and once dried onto a silicone substrate, they are inherently brittle and will flake off after repeated bending of the elastomer.

One research group has tried modifying the surfaces of polymer substrates by adding sulfonated or phosphvinyl-grouped polymers and then immersing these in calcium phosphate aqueous solutions (Dal88a, Dal88b, and Dal91). The presence of phosphate groups on the surface of the substrate has induced the precipitation of hydroxyapatite (Dal91) and the sulfonated surfaces were strong adsorbents of calcium ions (Dal88a). Polymers were saturated with calcium prior to immersion and would induce the formation of crystals of calcium carbonate monohydrate, but not hydroxyapatite or tricalcium phosphate (Dal88a).

A method detailing the precipitation of bonelike calcium phosphate and hydroxyapatite films on a variety of substrates has been introduced (Abe90). This method involved the attachment of a substrate in a face-to-face orientation to a bioactive glass plate. Alumina spacers maintained a constant distance of 0.5 mm between the substrate and glass plate. This combination was immersed in a simulated body fluid (SBF) for 7 days, separated, gently washed with ion-exchange and distilled water, and dried. Re-immersion of the substrate in a solution containing 1.5

times the ion concentrations as SBF (1.5SBF) for an additional 7 days, caused the formation of a continuous apatite layer (1 μm thick) on the surface that had been facing the bioactive glass. Increasing the distance between the substrate and glass during the first immersion reduced the amount of apatite formed and no apatite was formed at a distance greater than 2 mm. The authors concluded that the mechanism of apatite coating was 1) silicate ions dissolving from the glass and adsorbing on the substrate, 2) apatite nucleation on the adsorbed silicate ions, and 3) apatite nuclei growth on the substrate by using ions from the SBF (Abe90). Distinct uncoated areas were present in the location of where the alumina spacers had been during the first treatment.

A refinement of the technique by the same group included placing the substrate on a bed of bioactive glass particles during the first immersion in SBF. This process was described as a "Biomimetic Method" (Tan94, p. 2205) for forming a bonelike apatite layer. The authors tested the adhesive strength of a bonelike apatite layer grown on 10 different types of polymer substrates. The first immersion, face down on top of glass particles, was in SBF for 6 days and was followed by a second immersion, without glass particles, in the 1.5SBF solution for an additional 6 days.

If the first step was omitted, the apatite did not form during the second treatment (Tan94). Although silicone was included as one of the polymers to be tested, data on the adhesive strength or the coating process was omitted from the discussion (all other polymers were included) (Tan94). No reason for this omission was given by the authors. The polymers which showed the greatest adhesive strengths were polyethylene terephthalate (PET) and polyarylether sulfone (PESF); the authors attributed this strength to chemical bonding between the apatite layer and the polymer's ester and sulfonyl groups, respectively (Tan94). The proposed mechanism of apatite coating on the substrate was the same as discussed in the previous publication (Abe90). Small increases in the adhesive strength could be made for polymers such as PET and polymethyl methacrylate if the substrate were pretreated in 1 N HCl prior to the first step (Tan95). This pre-treatment increased the number of polar groups on the surface of the substrate as measured by X-ray photoelectron spectroscopy (XPS) (Tan95). These polar groups were intended to improve the bonding of apatite to the surface. Although the use of bioactive glass powder eliminated the uncoated areas where alumina spacers had been in the previous study (Abe90), only 1 side of the substrate was coated with the thin (< 5 μm) apatite layer (Tan94).

One technique to coat the entire implant is a pulsed laser deposition discussed in a recent study (Zab94). A thin amorphous film of HAP was applied to the surface of a silicone tubing. The film was measured between 0.5 to 1 μm in thickness and could be applied to a selected area (Zab94 and Zab95). The coating was continuous, except for cracks that formed when the tubing was bent. It is unclear how this cracked, amorphous and extremely thin coating will react in a percutaneous application.

2.2.4 Attempts at Sol-gel Coating

Several unsuccessful attempts were made in our lab to coat silicone with a layer of sol-gel derived bioactive glass. A bioactive glass sol was made by mixing Tetra(ethoxysilane) (TEOS), Triethyl phosphate, Calcium nitrate pantahydrate, Nitric acid, distilled water and ethanol using a formula published by Li (Li91b). The coating of silicone with sol-gel derived bioactive glasses suffered from two major difficulties. 1) the sprayed on hydrophilic sol left very tiny islands of glass on the surface of a cured silicone sheet rather than an even coating; further, these islands inherantly had a large curvature and surface area, complete dissolution of the islands was observed in as short a time as 12 hours in water at 37°C, 2) the high acid content of the sol interfered with

[illegible] curing of the silicone when mixed with two-part [illegible] this resulted in bubbles and voids in the sheeting. In an act of desperation, melt-derived bioactive glass (Bioglass® 45s5, 710-90 µm powder, U.S. Biomaterials, Alachua, FL) powder was pressed into the surface of a silicone sheet 2 hours into the curing reaction. The results of *in vitro* testing of these samples, called "5/5/press", showed the formation of HCA both on the glass particles and between the particles on the silicone surface. These results concurred with those of other researchers at about the same time. Investigators found that PESF/bioactive glass composite surfaces could precipitate HAP both on the glass reinforcing phase and the polymer between the glass phase (Ore95 and Mar96).

CHAPTER 3
MATERIALS AND METHODS

3.1 Preparation of Silicone Sheets

Silicone sheets were made by casting a solution of part silicone (Shin-Etsu KE-1935, Lot 40716i, Shincor Silicone Inc , Akron, OH)in hexane onto a glass plate and then curing the silloone in a vacuum oven A 1:1 ratio siiicone/hexane solution is made by weighing 12.5 g of each siilcone part into a 50 cc disposable centrifuge tube (Flaherbrand®, Fisher Scientific, Pittsburgh, PA)and then mixing this with 25 mL of hexane (Optima grade, Fisher Scientific, Fair Lawn, NJ) on a rotary mixer for 1 hour. This siiicone/hexane solution was poured onto a glass plate (12 in x 6 in) that had a border made of disposable glass pipet glued to the plate with commercial siiicone caulk The hexane was allowed to evaporate in a hood at room temperature and then the plate was placed in a vacuum oven (National Appliance Co., Portland, OR) pumped down to 10 Torr for 1 hour and then held at 10 Torr over-night at 70°C The first hour of pumping insured that all entrapped air was

removed from the silicone. The resulting sheet of silicone was removed from the glass plate and cut into smaller squares (5 cm x 5 cm) for coating with bioactive powder.

3.2 Preparation of Buffers

Two types of buffers were made and used during the *in vitro* testing of these samples: 1) a simulated body fluid (SBF) buffer and 2) a Tris buffered solution. The SBF was described by Kokubo for the *in vitro* testing of bioactive glasses (Kok90a) as having similar ion concentrations and pH as human blood plasma. The SBF was buffered to pH 7.25 with tris(hyroxymethyl) aminomethane (THAM) and hydrochloric acid (HCl) at 37°C. The SBF was made by adding the reagents, shown below in Table 3-1, to 4 L of ultra-pure water.

Table 3-1: Reagents used for preparing 4 L of SBF.

Reagent	Amount
NaCl	31.984 g
$NaHCO_3$	1.400 g
KCl	0.896 g
K_2HPO_4	0.696 g
$MgCl\ 6H_2O$	0.812 g
1N - HCl	160 mL
CaCl	1.112 g
Na_2SO_4	0.284 g
$NH_2C(CH_2OH)_3$ (THAM)	24.228 g

Once the reagents are dissolved and the solution is brought to 37°C, the pH is adjusted to 7 25 by adding very small amounts of either THAM or 1 N HCl. Tris buffer solutions were made by using only THAM and HCl.

3.3 Coating Methods

3.3.1 Basic Coating of Silicone Sheets

Mixing of a sample of two-part silicone as described in section 3 1 was followed by placement in a vacuum oven with pumping down to 10 Torr at 70°C for 1 hour to remove the entrapped air bubbles. Then 5 g of bioactive glass powder (45s5 Bioglass®, 710-90 µm diameter, Lot# V10X, U S Biomaterials Inc , Alachua, FL) was spread with a glass microscope slide onto the silicone surface. The powder was pressed into the tacky, partially cured surface gently with the glass slide and the glass plate placed back into the vacuum oven under 10 Torr of vacuum at 70°C for 24 hours. A rectangular piece of this sample (1 cm by 2 cm) was exposed to 30 mL of SBF at 37°C for 10 days. After that period, the sample was removed, rinsed with acetone, and allowed to air dry at room temperature in a desiccator. The surface of the reacted samples was analyzed using Fourier Transform Infrared (FTIR) spectroscopy using a diffuse reflection

stage. Part of the reacted sample was coated with gold/palladium and imaged using low voltage (2 keV) scanning electron microscopy (SEM).

Varied amounts of powder

Seven squares, 5 cm by 5 cm, were cut from a piece of silicone sheeting prepared using the technique described section 3.1. These squares were soaked in hexane for 2 hours to remove most of the oils in the sheeting. Once dry, the squares were placed flat on a clean glass plate. A solution of two-part silicone/hexane was made by weighing out equal amounts of each part of silicone into a centrifuge tube and then adding enough hexane to make a 10% (silicone weight/ hexane volume) solution. This 10% silicone/hexane solution was allowed to mix on a tube rotator for 1 hour. Using a 1 mL glass pipet, 1 mL of this solution was applied evenly to the surface of each silicone square and the hexane allowed to evaporate. This produced a thin layer of uncured silicone on the surface of each square. A weighted amount (0.0, 0.1, 0.2, 0.3, 0.4 and 0.5 g) of bioactive glass (45s5 Bioglass®, 125-53 μm diameter, Lot# VIOX) powder was evenly applied to each square using a "salt shaker"-like device made of a GFC vial (National Scientific Co., Lawerenceville, GA) with several holes (1 mm each) punched into the Teflon septa. Each square was then placed between two Teflon

sheets and pressed in a heated Carver press at 150°C to 5000 psi for 1 hour. The seventh sample, labeled 6B, was coated with the thin layer of uncured silicone and 0.5 g of glass powder using the above technique but, was heated in a vacuum oven at 10 Torr and 70°C for 24 hours and not pressed. Cross-sectional micrographs were taken of samples from each square using SEM. Cross-sectional samples from each square were broken after freezing in liquid nitrogen for 2 minutes. Sixteen disks, 1 cm diameter, were cut from each square using a standard cork-borer. These disks were then placed in 15 mL centrifuge tubes (Fisherbrand®). At the appropriate time, 8 mL of SBF was added to each tube, the tube sealed and placed in a constant temperature shaker bath (American Optical, Model 406015, Buffalo, NY) at 37°C. One tube was removed at 10 minutes and 1, 2, 6, and 20 hours. This provided a coated surface area to solution volume (SA/V) ratio of 0.1 cm^{-1}. After samples were reacted, they were removed from the SBF with tweezers, submerged in acetone (Optima grade, Fisher Scientific, Fair Lawn, NJ) for 1 minute, gently removed, allowed to air dry at room temperature on a lint-free tissue (Kimwipes EX-L, Kimberly-Clark Corp., Roswell, GA) and placed in labeled petri dishes. The solution was replaced in the temperature bath for 1 hour to return to 37°C and the pH of the solution

measured with a probe that had been calibrated using pH standards that were also at 37°C. Measurement was carried out while still in the constant temperature bath, then the solution was sealed and saved for inductively coupled plasma (ICP) spectroscopy analysis for the elemental concentration of phosphorus (P), silicon (Si), and calcium (Ca) in solution. The reacted surface of each disk was analyzed using FTIR.

Test of 'Halo' effect

Three squares, 5 cm by 5 cm, were cut from a silicone sheet, soaked in hexane, dried, and placed on a clean glass plate as described above. A 10% (W/V) silicone/hexane solution was made and allowed to mix on a tube rotator for 1 hour. Using a 1 mL glass pipet, 0.5 mL of this solution was applied evenly to the surface of one silicone square and the hexane was allowed to evaporate. This produced a thin layer of uncured silicone on the surface of each square. Sixteen disks, 1 cm diameter, were cut from this coated sheet. A short piece of glass tubing, 0.5 cm internal diameter, was gently placed in the center of a coated disk. Bioactive glass (45s5 Bioglass®, 125-53 μm diameter, Lot# V10X) powder was placed down the short glass tube. A vacuum was applied to the glass tube, using a vacuum pump and a rubber hose, to remove any unattached bioactive glass particles. The glass

was gently [illegible] cm diameter section of bioactive glass coated silicone in the disk's center. This procedure was repeated for each disk using a new glass tube each time. The disks were placed on a glass plate and cured in a vacuum oven at 10 Torr and 70°C for 24 hours. These samples were labeled "C13". To the other two squares, 0.1 mL of the 10% silicone/hexane solution was applied to a 0.5 cm wide section of two sides of each square. The remainder of the square was masked from coating by placing a glass microscope slide on the surface of the square. The hexane was allowed to evaporate and bioactive glass powder, as in C13, was dropped onto the uncured silicone area. The squares were then placed in a vacuum oven at 10 Torr and 70°C for 24 hours. After the silicone cured, the glass microscope slides were removed from the squares and excess bioactive glass powder was rinsed from the squares with acetone. From each of these two squares, 8 samples were cut in the shape of rectangles 1 cm by 2 cm with a bioactive glass coated end that measured 1 cm by 0.5 cm. These rectangular samples were labeled "R13". A diagram of each of these samples is shown in Figure 3-1. Both sets of samples were placed in 15 mL centrifuge tubes for bioactivity testing. At the appropriate time for samples at 0, 1, 5, 10, and 20 days, 8 mL of SBF was added to each tube

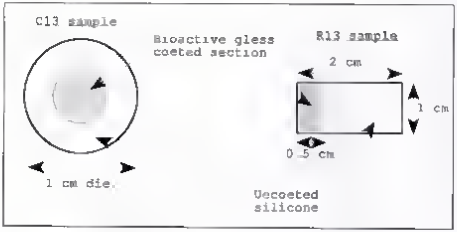

Figure 3.1: Diagram of C13 and R13 samples

containing a C13 sample and 15 mL of SBF was added to tubes containing a R13 sample. The tubes were sealed and placed in a constant temperature shaker bath at 37°C (3 samples at each time period). These seperate SBF volumes maintained a coated surface area to solution volume (SA/V) ratio of 0.1 cm

After samples were reacted, they were removed from the SBF, submerged in acetone for 1 minute, removed and allowed to dry on a lint-free tissue. The solution was replaced in the temperature bath for pH measurement of the solution at 37°C. The solution was sealed and saved for ICP analysis. The reacted surface of each sample was analyzed using FTIR spectroscopy and low voltage SEM.

Fine bioactive glass powder

Six squares, 5 cm by 5 cm, were cut from a sheet of silicone, soaked in hexane, dried, and placed on a glass plate as described above. Using a micropipetar (Oxford Samplar, Oxford, Inc., St. Louis, MO) 0.15 mL of a 10% silicone/hexane solution was applied to one end of 3 squares and spread across each square using a glass microscope slide. Once the haxane evaporated, a very thin layer of uncured silicone remained on each of the 3 squares. The following 3 sizes of fine bioactive glass powder (U.S. Biomaterials, Alachua, FL) were applied to each to both an uncoated square and a coated square: 1) 45s5 Bioglass®, <20 µm powder, Lot# 9160; 2) 45s5 Bioglass®, <5 µm powder, Lot# 9160; and 3) 45s5 Bioglass®, <2 µm powder, Lot#9160. The glass powder was spread onto each square using a glass microscope slide. All 6 squares were then placed in a vacuum oven at 10 Torr and 70°C for 24 hours. Disks, 1 cm diameter, were cut from each of the squares and placed in labeled 15mL centrifuge tubes. At the appropriate time, 8 mL of SBF was added to each tube containing, the tube sealed and placed in a constant temperature shaker bath at 37°C for 0, 1, 3, 12, and 24 hours (3 samples at each time period). In addition, 3 disks of uncoated silicone were reacted in 8 mL of SBF at 37°C for 3 and 24 hours. After samples were

reacted, they were removed from the SBF, submerged in acetone for 1 minute, removed and allowed to air dry at room temperature on a lint-free tissue. The solution was replaced in the temperature bath for pH measurement of the solution at 37°C. The solution was sealed and saved for ICP analysis. The reacted surface of one sample from each type was analyzed using FTIR diffuse reflection spectroscopy.

3.3.2 Mesh Coating of Patterns

Spectra/Mesh® woven nylon mesh pieces (Spectrum Medical Industries, Inc., Houston, TX), commonly used for filtration, were used to mask the surface of silicone squares coated with uncured silicone providing a pattern of powder on the surface of the silicone squares.

70 mesh

One square, 5 cm by 5 cm, was cut from a sheet of silicone, soaked in hexane, dried, and placed on a glass plate as previously described. Using a micropipetor 0.15 mL of a 10% (W/V) silicone/hexane solution was applied to one end of the square and spread using a glass microscope slide. Once the hexane evaporated, a piece of 70 µm Spectra/Mesh® (Lot# 00450, 70 µm square holes separated by 70 µm wide threads of nylon), 5 cm by 5 cm, was gently applied on top of the uncured silicone layer. Bioactive glass powder (45s5

Bioglass®, 125-53 μm diamatar, Lot# VIOX) was spread onto this masked surface. Once the glass powder had filled all of the pores in the mesh, the excess glass was gently blown off using compressed dry air. The nylon mesh was removed leaving a pattern of single glass particles evenly spaced. The square was placed in the vacuum oven at 10 Torr and 70°C for 24 hours. Disks of 1 cm diameter were cut from this square and placed into 15 mL centrifuge tubes. Eight millilitars of SBF was added to each tube. The tube was sealed and placed in a constant temperature shaker bath at 37°C for 0, 1, 3, 7, 12 and 24 hours (2 samples at each time period). In addition, single disks were reacted in SBF for 1, 2, 3 and 10 days at 37°C. After samples were reacted, they were removed from the SBF, submerged in acetone for 1 minute, removed and allowed to dry on a lint-free tissue. The pH of the solution was measured at 37°C, the solution saved for ICP analysis, and the reacted surfaces analyzed using FTIR spectroscopy and low voltage SEM.

<u>70/45, 70/52, 70/55, & 70/60 samples</u>

Using the same technique described in <u>70 Mesh</u> above, 2 squares each were coated with a pattern of the following bioactive glass powders: 1) 45s5 Bioglass®, 125-53 μm diameter, Lot# VIOX, 2) 52s Bioglass®, 90-53 μm diameter, Lot# 9160, 3) 55s Bioglass®, 90-53 μm diameter, Lot# 9160,

[redacted] Bioglass®, >90 µm diameter, Lot# 5160. These glass powders are of different composition and exhibit different reactions *in vivo*. The coated squares were placed in a vacuum oven at 10 Torr and 70°C for 24 hours. Disks of 1 cm diameter were cut from these squares and placed into labeled 15 mL centrifuge tubes. Disks were reacted with 8 mL of Tris buffer and SBF at 37°C for 3, 7, 9, 10 and 12 hours in a constant temperature shaker bath. In addition, 2 uncoated 1 cm disks were also reacted in SBF at the same time periods. The reacted samples were removed from their solutions, submerged in acetone for 1 minute, removed and allowed to dry on a lint free tissue. The pH of the solution was measured at 37°C, the solution saved for ICP analysis, and the reacted surfaces analyzed using FTIR spectroscopy and low voltage SEM.

3.2.3 Dip Coating of Catheters

Samples, 5 cm long, of an all-silicone Foley catheter (16 French, Bard Access) were cut and then washed in hexane for 2 hours (excluding the balloon and distal ends). After the catheter pieces were allowed to dry, they were placed in a 50 mL centrifuge tube that contained 30 mL of a 25% (W/V) silicone/hexane solution (7.5 g of two-part silicone and fill with hexane to 30 mL). Two cathatar pieces were placed in this solution for 2 hours at room temperature. Then the

catheters were removed and placed on bent paper clips to allow the excess dipping solution to drip off and the hexane to evaporate (see diagram of process in Figure 3-2). After 1 hour, the ends of the catheter pieces are masked-off by placing tape around each end and crimping the tape-ends. The masked catheter pieces are then placed in a 15 mL centrifuge tube that containing 10 g of bioactive glass (45s5 Bioglass®, 125-53 μm diameter, Lot# V10X) powder. By rotating the tube parallel to the floor, all sides of the catheter are coated with powder. Once coated with powder, the catheter pieces were removed from the centrifuge tube and the tape carefully removed. The powder was pressed into the surface of the catheter piece by rolling it on a glass plate with a microscope slide. The catheter pieces were placed in GPC vials to hold them upright and heated in the vacuum oven at 10 Torr and 70°C for 24 hours. SEM images of catheter pieces broken with liquid nitrogen were taken to view the cross-section.

3.4 Surface Analysis

The reacted surface of each sample was analyzed using Fourier transform infrared (FTIR) spectroscopy and low voltage (2 keV) scanning electron microscopy (SEM).

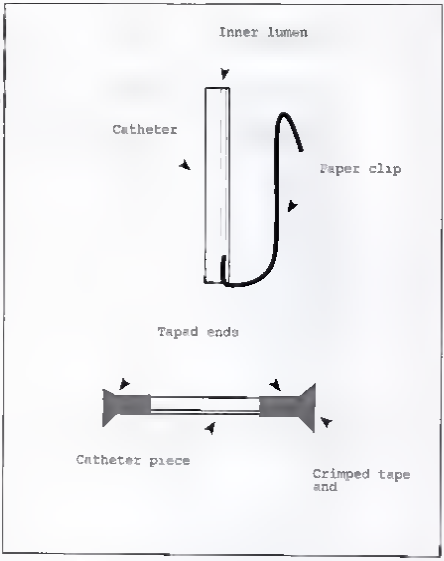

Figure 3-2: Diagram of methods used to hang and mask catheter pieces for dip coating with silicone.

3.4.1 FTIR

The surface of reacted samples was analyzed using Fourier transform infrared (FTIR) spectroscopy using a diffuse reflection stage (Model 205xb, Nicolet Instrument Corp., Madison, WI). Diffuse infrared reflectance was chosen due to the large amount of scattering induced by the irregular glass powder coating the surface of these samples, the poor IR transmission qualities of silicone, and the fact that this technique has been used by many researchers to study the reaction surfaces of bioactive glasses (Cla90, Kok90b, Hen91, and Gre95). Samples were placed on the diffuse stage and the IR beam focused for the best reflection intensity.

3.4.2 SEM

Half or quarter pieces of each reacted sample were cut with a scalpel blade and mounted on aluminum SEM stubs with cyanoacrylate glue (SuperGlue®). Samples were grounded to the stubs by using carbon paint and the stub coated with a very thin layer of gold/Palladium using a sputter coater (2 minutes coating time). Samples were analyzed by low voltage (2 KeV) SEM (Joal JSM-6400, Bedford, MA) and representative photos of each surface were taken using Polaroid® Type 55 4x5 Instant Sheet film (Polaroid, Cambridge, MA).

3.5 Solution Analysis

3.5.1 Solution pH

After removal of the reacted sample, the solution was replaced in the temperature bath for 1 hour to return it to 37°C. The pH of the solution was measured (Corning pH Meter, Model 320, Corning, NY) with a probe (Accumet Combination Electrode, Fisher Scientific, Atlanta, GA) that had been calibrated using pH standards (Fisher Scientific, Atlanta, GA) at 37°C.

3.5.2 Elemental Concentrations

The elemental concentrations of phosphorus (P), silicon (Si), and calcium (Ca) in solution were measured using inductively coupled plasma (ICP) atomic emission spectroscopy using a Plasma 40 (Perkin-Elmer, Norwalk, CT) ICP is an atomic emission technique that measures the concentration of elements in an aqueous solution by using a plasma torch to ignite a fine mist of solution. The solution sample was introduced into the instrument through a capillary tube by means of a peristaltic pump. A nebulizer converts the liquid to a fine aerosol which is sprayed into the plasma. The spectrum of light emitted from this ignition is characteristic of the elements in solution.

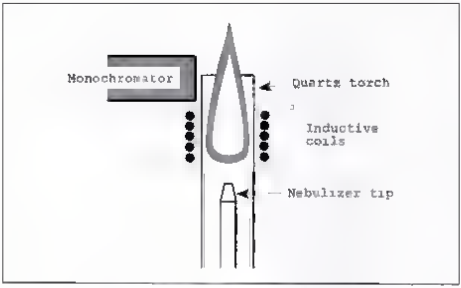

Figure 3-3 ICP torch confignration

Each element emits a unique set of wavelengths of light and the concentration of that element is directly proportional to the intenelty of those emitted waveiengths By using standard concentration solutione and careful volumetric dilutions, a standard curve relating the intensity to the concentration can be plotted

An ICP method was created to measnre the concentrations of elemental P, Si end Ca in solutions reacted with coated silicone samples. The emission wavelengths of each element were chosen from established tables (Kel59), photomultiplier tube (PMT) voltages and element scan times that insured accurate measurement Parameters are shown in Table 3-2.

Table 3-2| ICP parameters used

Element	Wave length (nm)	Element time (msec)	PMT voltage (V)
Phosphorus	213 62	1008	600
Silicon	288.16	800	600
Calcium	393 37	1008	300

Two standard solutions were made using 1000 ppm Spex Plasma standards (Spex Chemical, Metuchen, NJ) of phosphorus (Lot No 5-31CA), silicon (Lot No 4-28ASI) and calcium (Lot No. 4-28OP). Standards were made using class A volumetric flasks and pipet, diluted with ultra-pure water. Standards consisted of 100 and 50 ppm P; 100 and 10 ppm Si, and 200 and 100 ppm Ca. A blank solution of ultra-pure water was also used. Standards and the blank were run and the instrument calculated a linear standard curve (intensity vs. concentration). Correlation coefficients of these standard curves varied between 0.994 and 0.999. The concentrations of each element in solution was calculated using these standard curves and reported as ppm. Three measurements were taken of each solution and the mean and standard deviation calculated and reported by the instrument. When the blank was run as a sample the values obtained were 0.3 ppm P, 0 ppm Si, and 0 ppm Ca. Detection limits cited for these are 0.2 ppm P, 0.01 ppm Si, and 0.2 ppm Ca (Kel59).

CHAPTER 4
RESULTS AND DISCUSSION

4.1 5/5/Press

After the number of failed attempts at coating silicone with sol-gel derived bioactive glass, it was a pleasant surprise to find that a coating made of melt-derived glass powder (named "5/5/Press") was both stable in a simulated body fluid (SBF) buffer for 10 days and formed an apatite layer on the surface. Analysis of the reacted surface, by Fourier transform infrared (FTIR) spectroscopy, showed that a hydroxycarbonate apatite (HCA) layer had formed on the surface after 10 days reaction (see Figure 4-1). Figure 4-1 shows a comparison between FTIR spectra obtained from the bioactive glass powder coated sample and an uncoated silicone disk reacted in SBF for 10 days at 37°C. The spectrum from the coated sample (top spectrum) show the characteristic peaks of a HCA layer on the reacted surface: 3 narrow peaks near 610, 574, and 566 cm^{-1} and a broad peak at 1050 cm^{-1}, representing the P-O crystalline bending vibration and P-O stretching vibration, respectively.

(Hen91) The uncoated sample (bottom) shows a result for silicone: a narrow peak at 1250 cm^{-1} representing $Si-CH_3$ bending, 2 peaks at 1100 and 1000 cm^{-1} representing Si-O stretching, and a strong peak at 800 cm^{-1} representing the Si-O-Si tetrahedral bonding.

When the reacted surface of the 5/5/Press sample was imaged using low voltage (2 keV) scanning electron microscopy (SEM) an interesting result was seen. Not only did the HCA layer precipitate on the bioactive glass particles, but it also formed on the silicone polymer surface between particles of bioactive glass (see Figure 4-2). This result corresponded to observations by other researchers testing composites made of bioactive glasses and engineering thermoplastic (i.e. polyethylene and PESF) at the same time (Hua95, Ore95 and Mar96). The success of this simple coating technique, inspired a goal change from sol-gel derived coating to melt-derived powder coating of silicone surfaces. Glass powder used to coat the 5/5/Press samples was of a very coarse size (710 - 90 μm), resulting in a rough surface and large particles of glass could easily be brushed off the surface. An experiment was designed using a finer size powder (125 - 53 μm) and varied amounts of glass powder pressed into the surface of an uncured silicone layer spread onto a fully cured silicone sheet.

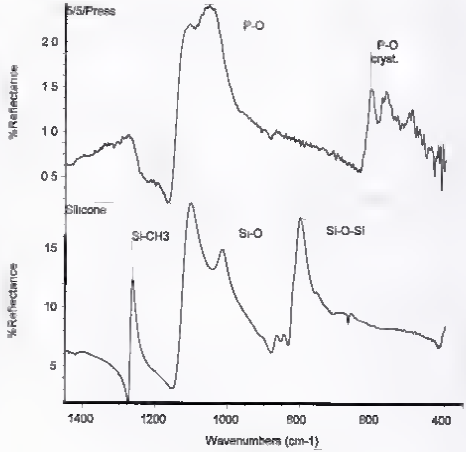

Figure 4-1 FTIR refection spectra for 5/5/Press bioactive glass powder coated silicone and an uncoated silicone disk reacted in SBF for 10 days at 37°C (compare with Table 2-2).

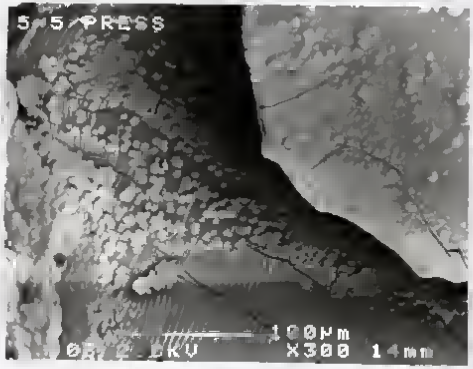

Figure 4-2: SEM micrograph of 5/5/Press surface reacted in SBF for 10 days at 37°C. Note that HCA (round hillocks) has formed on both the bioactive glass particle (left & right side) and the silicone polymer (middle).

4.2 Varied Amounts of Powder

[illegible]tive glass coated samples were made with 0, 0.1, 0.2, 0.3, 0.4 and 0.5 g of bioactive glass powder were tested in SBF for various times. Glass powder used on these samples was of a finer size range than before, 125 - 53 μm. The glass powder on these samples was pressed into a layer of uncured silicone applied to the surface and cured by using a heated carver press. In addition, a sample called "0S" was made without pressing, by adding 0.5 g of powder and cured using a vacuum oven. Figure 4-3 shows FTIR analysis of an uncoated silicone surface and a surface with 0.5 g of powder reacted for 20 hours in SBF at 37°C. Again the characteristic peaks of an HCA layer are present on the coated sample (bottom spectra) and not the uncoated sample (top). One of the silicone peaks can be observed in the 0.5 g sample, a peak at 1250 cm^{-1} for the $Si-CH_3$ bond vibration. The peak near 800 cm^{-1} on the bottom spectra may be due to Si-O-Si from the formation of a silica-gel layer during the reaction with SBF and not from the silicone polymer surface. A comparison of the amount of powder applied to the surface of samples reacted in SBF for 20 hours at 37°C is shown in Figure 4-4. The presence of a pair of peaks at 600 cm^{-1},

representing the P-O crystalline bending vibrations and the wide P-O stretching vibration near 1050 cm^{-1}, can be observed starting with 0.3 g sample and growing in strength with an increase in the amount of glass powder on the sample. Samples with 0.1 and 0.2 g of powder on their surface have little or no HCA is present (as represented by their FTIR spectra). Cross-section analysis of 2 samples imaged by low voltage SEM are shown in Figures 4-5 and 4-6. Cross-sections were made by breaking samples frozen in liquid nitrogen. Cross-sections of the 0.2 sample reveal that the majority of the bioactive glass particles are covered by silicone (particles in the center of Figure 4-5 are covered by a layer of silicone present to their right). This image is similar to what is observed with the 0.1 samples. Figure 4-6, shows a large number of particles exposed to the surface (top left of image) and is representative of what is observed with the 0.3, 0.4, and 0.5 samples. The results of this cross-sectional examination help explain the reasons for the differences observed in the FTIR analysis shown in Figure 4-4. Samples 0.1 and 0.2 present only a silicone surface. While, the 0.3, 0.4, and 0.5 samples present bioactive glass powder at their surfaces. SEM images of 20 hour reacted samples are shown in Figures 4-7 and 4-8.

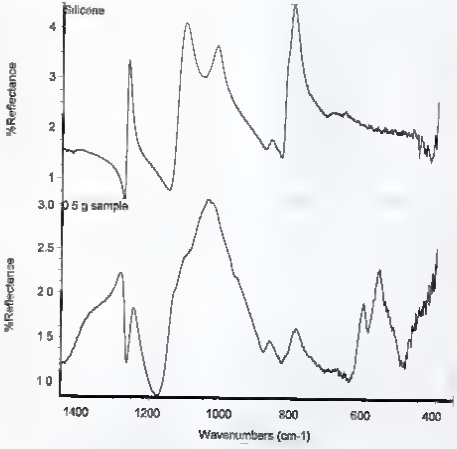

Figure 4-3 FTIR spectra of an uncoated silicone sample and a sample coated with 0.5 g of bioactive glass both reacted in SBF for 20 hours at 37°C

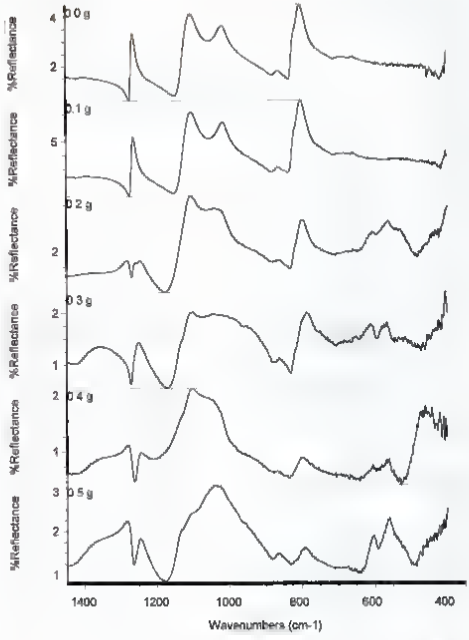

Figure 4-4 FTIR spectra of samples coated with 0, 0.1, 0.2, 0.3, 0.4, and 0.5 g of bioactive glass powder and reacted in SBF for 20 hours at 37°C.

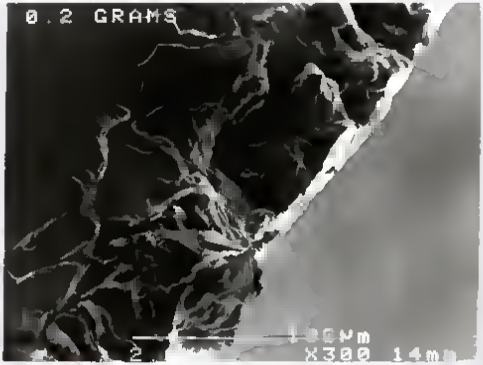

Figure 4-5: SEM image of the cross-section of a sample coated with 0.2 g bioactive glass powder (Showing particles covered by silicone layer)

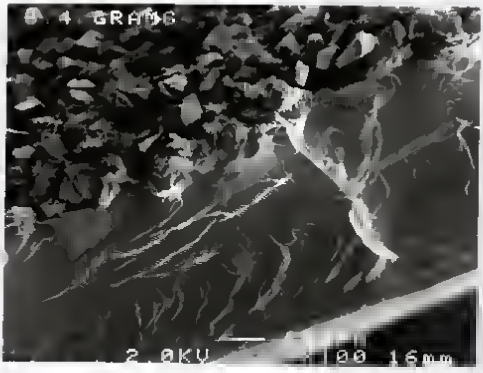

Figure 16 SEM image of the cross section of a sample coated with 0 4 g of bioactive glass powder. (Showing exposed particles on surface)

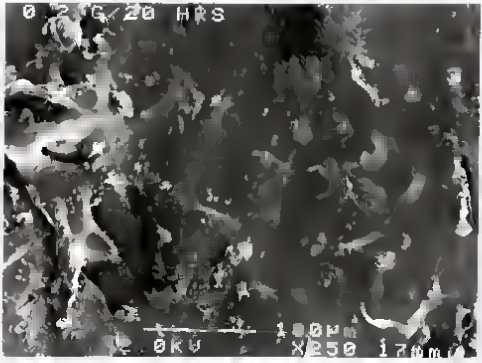

Figure 4 SEM image of the surface of a 0.2 sample reacted in SBF for 20 hours at 37°C. Note the lack of bioactive glass particles on the surface.

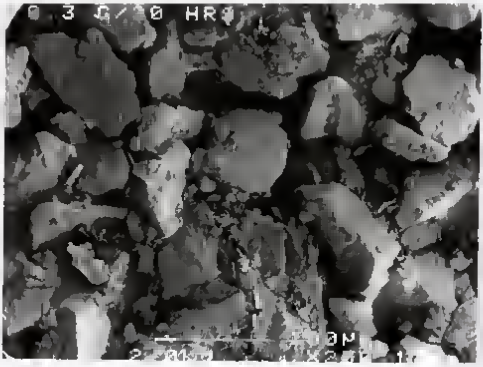

Figure 4.8 SEM image of the surface of a 0-3 sample reacted in SBF for 20 hours at 37°C. Note the large number of bioactive glass particles on the surface

Figure 4-7 shows the surface of a 0-2 sample reacted SBF for 20 hours at 37°C. This surface shows few exposed bioactive glass particles and little reaction at the surface. In contrast, Figure 4-8 shows the reacted surface of a 0-3 sample, many bioactive glass particles are observed and the surfaces of those particles show HCA nodules and growth. These results correspond to what is observed with FTIR spectra of these surfaces. If no bioactive glass particles are exposed then there is no reaction at the surface to produce an HCA layer. Composites made using bioactive glasses and engineering thermoplastics are traditionally polished with SiC sand paper to expose the underlying glass from the matrix polymer (Hna95 and Ore95).

This difference is also observed by the change in elemental concentrations of phosphorus (P), silicon (Si), and calcium (Ca) in each reaction solution analyzed by inductively coupled plasma (ICP) spectroscopy. Figures 4-9, 4-10, and 4-11 show the concentrations of P, Si and Ca in solution, respectively, plotted for each time period and sample. Figure 4-10 shows a considerable drop in the P concentration for the 0-3, 0-4, and 0-5 samples, to levels that are much lower than the original SBF concentration of 31.3 ppm. This phosphorus level reduction starts at the 2 hour time period and continues through the 20 hour period

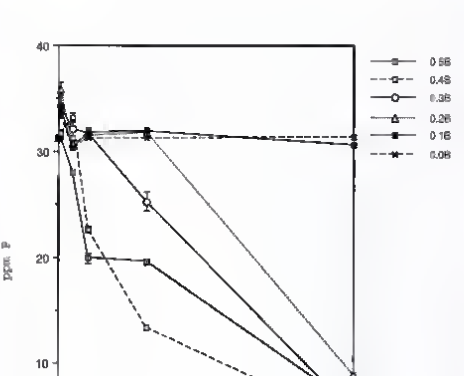

Figure 4-9: Plot of the phosphorus concentration (in ppm) in SBF solution reacted with 0, 0 1, 0 2, 0 3, 0.4 and 0 5 samples versus the time period (in hours) at 37°C.

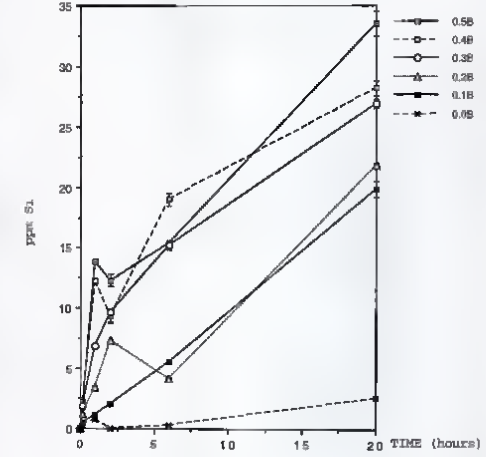

Figura 4.10: Plot of the silicon concentration (in ppm) in SBF solution reacted with 0, 0.1, 0.2, 0.3, 0.4 and 0.5 samples versus the time period (in hours) at 37°C.

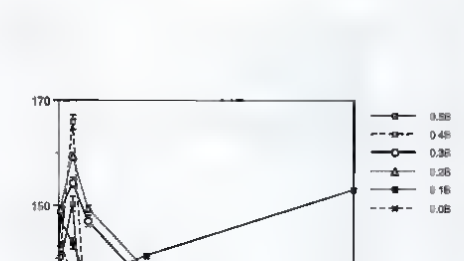

Figure 4-11: Plot of the calcium concentration (in ppm) in S&F solution reacted with 0, 0.1, 0.2, 0.3, 0.4 and 0.5 samples versus the time period (in hours) at 37°C.

This drop in the P level of reaction solutions has been associated, by many authors, with the precipitation and growth of an HCA layer on the surface of bioactive glasses (Kim89, Li89a, Kok92 and Oht92) and is preceded by an increase in the P level. This increase is associated with the leaching of phosphorus ions from the glass into solution. The observation of a drop in the P level beginning at the 2 hour reaction time period, was also reported by Kim et al., with 45s5 Bioglass® disks reacted in Tris buffer(Kim89). This trend is not observed with the 0, 0.1, and 0.2 samples, except for the single 20 hour 0.2 sample. For the rest, the phosphorus level remained at or near the original SBF level, indicating that there was no precipitation of HCA on the sample surface. In addition, the same trends are also observed with the Ca levels plotted in Figure 4-11. An increase in the Ca level at the 1 hour time period, followed by a decrease to a level far below the original level in the SBF solution (135.0 ± 2.2 ppm). This trend being observed only for the 0.2, 0.3, 0.4, and 0.5 samples. The 0.0 and 0.1 samples remain at or near the original SBF level. The increasing trends observed in Figure 4-10 show that Si leaches from all of the glass coated samples and the amount of silicon that leaches into solution is directly related to the amount of glass coated

on the surface. Even the 0.1 and 0.2 samples leach small amounts of elemental silicon in to solution, contrary to the observation with SEM that this glass is covered by the silicone layer. However, images of the reacted samples shown in Figure 4-7, reveal that the surface has many defects that could allow limited access of the solution to the underlying glass particles. The 0.3, 0.4, and 0.5 samples all leached Si into solution at similar rates and leached much more Si that the 0.1 and 0.2 samples. The leaching of Si into solution by a bioactive glass, resulting in the condensation and repolymerization of a silicon-rich gel layer at the surface of this glass has been theorized as a mechanism for accelerating the nucleation and growth of the HCA layer that forms both *in vitro* and *in vivo* (Hen93a).

4.3 Test of 'Halo' Effect

Marcolongo et al., described the HCA reaction layer that formed around bioactive glass fibers imbedded in a polysulfone composite as a "Halo" of bioactivity (Mar96). The authors reported that after 21 days *in vitro*, nodules of a calcium phosphate layer (3-5 μm thick) were observed using SEM in regions between 10 and 70 μm surrounding the bioactive glass fibers. The following experiments were

established to determine if this effect would also occur with silicone samples. Both circular (C13) and rectangular (R13) shaped samples were made and tested. These samples had distinct areas coated with bioactive glass powder and uncoated areas (see Figure 4-12).

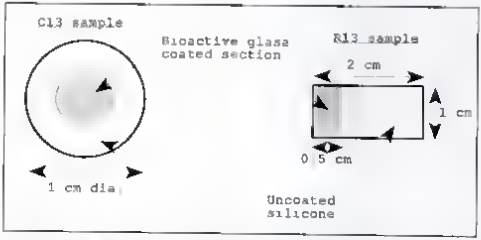

Figure 4-12: Diagram of C13 and R13 samples

Analysis of the surface, by FTIR, of C13 samples showed a similar result as the samples described in the previous section, an HCA layer formed on the surface after 1 day reaction in SBF (see in Figure 4-13). These results only examine the formation of an HCA layer on the center glass region. Low voltage SEM images revealed a new trend in the HCA formation (see Figures 4-14 through 4-17).

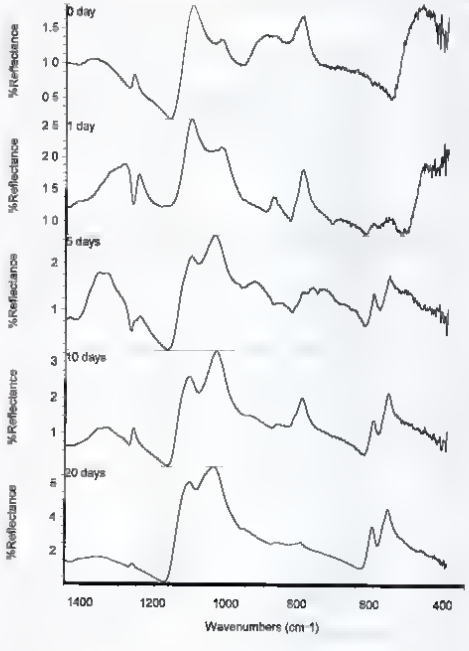

Figure 4-13 FTIR reflection spectra of the center of C13 samples reacted in SBF for 0, 1, 5, 10 and 20 days at 37°C.

Figure 4-14 SEM micrograph of a section of C13 sample reacted in SBF for 20 days at 37°C. Note the lack of HCA growth on the silicone surface away from closely packed bioactive glass particles. A layer of HCA can be seen coating the particle surfaces

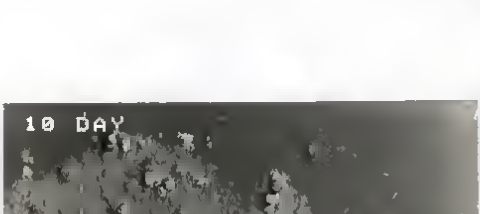

Figure 4-15 SEM micrograph of a section of C13 sample reacted in SBF for 10 days at 37°C. Note that on the left, where glass particles are spread out, there is extensive growth of the HCA layer on the silicone surface. Growth is limited on the right, where particles are closely packed together

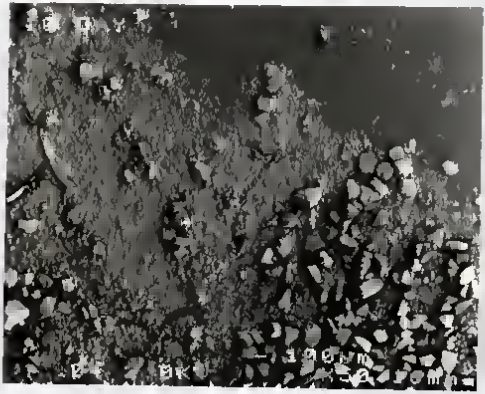

Figure 4-16 SEM micrograph of a section of C13 sample reacted in SBF for 10 days at 37°C. This is a magnified version of Figure 4-15.

Figura 4-17 SEM micrograph of a section of C13 sample reacted in SBF for 5 days at 37°C. Note the layer of HCA grown both on and between the glass particles

The SEM micrographs shown in figures 4-14 through 4-17, show a pattern of broad HCA formation on silicone that has bioactive glass particles spread apart and HCA formation limited to only the particle surface for closely packed particles. These results lead to a new theory that governed the formation of HCA between bioactive glass particles (or regions). As the bioactive glass particles leach ions into solution, there forms a zone of leached ions around each particle. This leach zone is highly saturated with respect to phosphorus, silicon and calcium containing ions. If the particles are too close together leach zones overlap early in the bioactive reaction causing precipitation of silicon and then HCA on the surface of the particles only. If the particles are too far apart then the zone grows until silicon and then HCA precipitate only on the particle. If the bioactive particles are spaced just the right distance apart, then the separate leach zones for each particle grow until they overlap, at that point the solution is supersaturated, silicon and the HCA precipitate on both the particles and between the particles. In addition, the release of cations such as Na^+ and Ca^{2+} into the solution surrounding a glass particle through an ion exchange process, causes a localized increase in pH, this pH increase favors the precipitation of amorphous apatite (Fee79, Kou87

and Bro91a). This new distance theory of HCA formation between particles is being presented for the first time in this dissertation and is illustrated in Figure 4-18. This theory may explain trend that has been observed with composites made of bioactive material and thermoplastic engineering resins. When composites are made with <20% bioactive material, HCA is seen to form in vitro on the surface of the bioactive material and rarely on the substrate surface (Hua95 and Wan95). When higher concentrations of bioactive material are used, HCA forms over the entire sample surface. Examination of SEM micrographs published by these authors suggests that in composites made with <20% bioactive material, the particles (or regions) of bioactive material are spaced far apart from one another (Hua95 and Wan95). Samples with higher amounts of bioactive material showed particles that were close together. This theory may become important in composites made of bioactive material where the design of the device required maximum bioactivity at the surface with the least amount of bioactive filler material. Since the bioactive glass is the brittle phase of the composite, this would give a the desired tissue response while limiting the reduction in tensile strength and fracture toughness. A balance of properties is the ultimate goal of any composite material

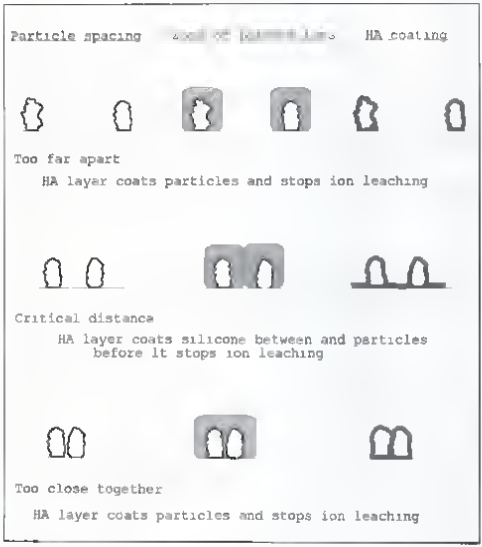

Figure 4-18: Diagram of HCA precipitation distance theory

The variation of pH with distance from bioactive glass materials was presented in a recent study (DeA96). These authors studied various bioactive glasses and glass-ceramics by measuring the pH using a pair of ion-sensitive field effect transistors (ISEFT) in direct contact with the material while immersed in SBF. An increase in the local pH, due to ion exchange, was observed after just 1 minute of immersion time for all the bioactive glasses. When the ISEFT was moved away from the interface, the measured pH decreased to the original value of the SBF (DeA96). This decrease occurred at a point < 1 mm from the surface of the bioactive glass and suggests that the ion exchange reaction is limited to the glass-SBF interface. The authors concluded that, since a higher pH favors HCA formation, the localized increase in pH at the glass-SBF interface determines the partial solution of silica and the subsequent precipitation of HCA (DeA96).

The elemental concentrations of Ca, P and Si in solution as measured by ICP are shown in Figure 4-13. The points on each graph represent the mean of solutions from 3 separate samples (3 measurements each) and the error bar represents the standard deviation of that mean. As in the previous study, after 1 day the phosphorus level has decreased due to the precipitation of the HCA layer

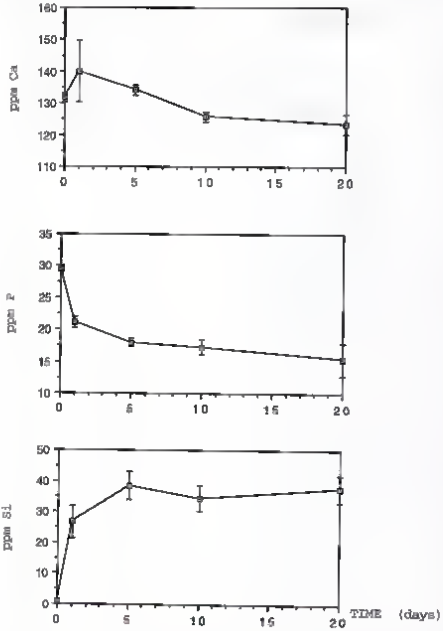

Figure 4-19 Plots of the elemental concentrations of calcium, phosphorus, and silicon in solutions of SBF reacted with C13 samples.

The Ca level also decreased below the original SBF value due to the HCA precipitation. The elemental Si concentration increases from 0.1 to a level near 35 ppm and remained at that level, suggesting that once the HCA layer precipitates on the surface of the glass particles the leaching of Si into solution is significantly reduced.

Uncoated silicone 1 cm disks that were reacted in SBF at 37°C for the same time periods showed no HCA formation by FTIR (Figure 4-20) or SEM (Figure 4-21). All R13 samples, due to their manufacturing process, had close packed particles at the silicone/glass transition. These samples all reacted similar to those areas that had close packed particles. SEM images were similar to Figure 4-14. FTIR and ICP analysis were omitted for these R13 samples.

4.4 Mesh Samples

To further test the theory described in Figure 4-18, samples of silicone were coated with a pattern of individual bioactive glass particles evenly spaced apart. Using a standard woven filtration mesh as a mask on the silicone surface, particles were allowed to contact the silicone surface only through the open areas on the mesh. An SEM micrograph image of a bioactive glass coated sample surface prepared in this manner is shown in Figure 4-22.

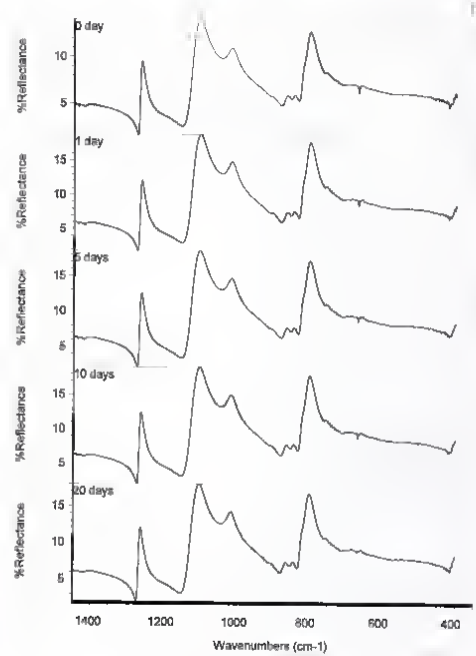

Figure 4-20 FTIR reflection spectra of uncoated silicone samples reacted in SBF for 0, 1, 5, 10 and 20 days at 37°C

Figure 4-21 SEM micrographs of uncoated silicon samples reacted in SBF for A) 5 days and B) 10 days.

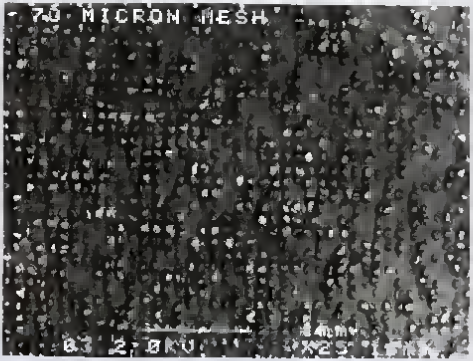

Figure 4-22 SEM micrograph of a sample made using a 70 μm filtration mesh as a mask. Note the evenly spaced glass particles on the surface

The majority of the surface in Figure 4-22 has single bioactive glass particles evenly spaced apart in rows. This sample was made using a very thin layer of uncured silicone, 45s5 Bioglass® (125-53 μm diameter), and a nylon 70 μm woven mesh (thickness 70 μm and 45% open area). A series of combinations of uncured silicone thickness, mesh size and particle size led to this coating method. If too thin a layer of uncured silicone was used, then the particle on the surface would dissolve away into the SBF during reaction. If too large a mesh size were used, then the sample would have small clusters of particles on the surface and reaction would be limited to only those clusters and not the silicone surface between the clusters.

Initial bioactivity testing included single samples tested at 1, 2, and 3 days in SBF at 37°C. SEM images of the surface of these '70 Mesh" samples revealed HCA growth both on the bioactive glass particles and the silicone between them (shown in Figures 4-23, 4-24, and 4-25). This result was observed if the particles were less than 100 μm apart. When individual particles were missing from the pattern, the HCA layer was not present on the silicone between the particles (see Figure 4-23). When two particles bordered an area with a missing particle, a bridging arc of HCA formation would be observed (center of Figure 4-24).

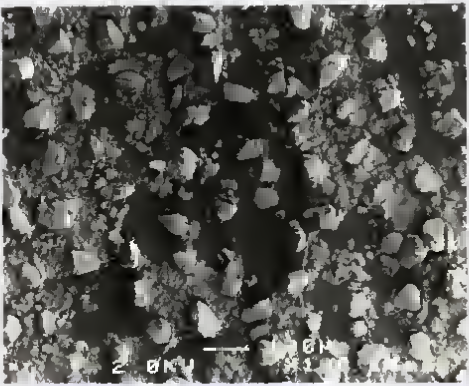

Figure 4-23 SEM micrograph of a 70 Mesh sample reacted in SBF for 3 days at 37°C. HCA layer can be seen between particles that are <100 μm apart.

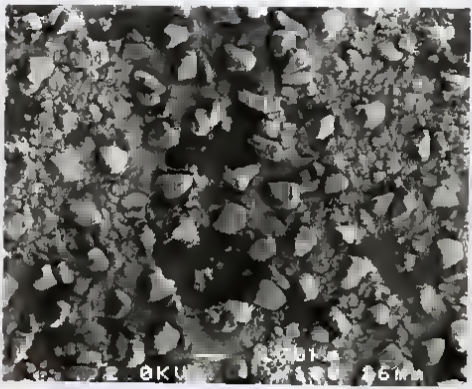

Figure 4-24. SEM micrograph of a 70 Mesh sample reacted in SBF for 3 days at 37°C. HCA layer can be seen between particles that are <100 μm apart. A circle of HCA can be seen on the border of a open area where a missing particle has caused a lack of HCA precipitation on the silicone surface.

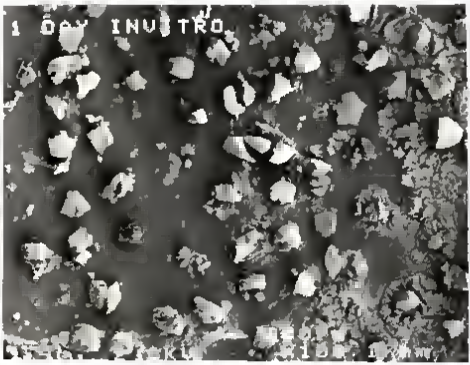

Figure 4-25: SEM micrograph of a 70 Mesh sample reacted in SBF for 1 day at 37°C. HCA layer can be seen beginning to form between particles in the upper left hand corner

The center area of Figure 4-24 is barren of HCA and the border of that area is circled by an arc of HCA. Figure 4-25 shows a 70 Mesh sample that has been reacted for 1 day in SBF, in the upper-left hand corner there can be seen the beginnings of HCA precipitation between particles that are with in the 100 μm range. This is in stark contrast to the HCA formation that has occurred on the right side of the image. On the left side there is a cluster of 3 particles almost touching each other. The close proximity of these 3 particles may be a contributing factor to difference between the two sides. This same trend can be seen with the line of 3 particle in the top center of the image, these have also just started precipitating between them and the particles above them. FTIR images of the surface of these reacted samples are shown in Figure 4-26. At 3 days, the surface showed little HCA on the surface as measured by the presence of a pair of P-O crystalline peaks at 610 and 574 cm^{-1}. This results because <45% of the surface of the sample is covered by bioactive glass particles. The rough surface of the particles and HCA growth areas scatter the light more in comparison to the smooth silicone which has more specular reflection and allows more of the silicone signal to reach the detector, giving a false reading of more silicone than HCA. Uncoated silicone showed greater FTIR reflection-

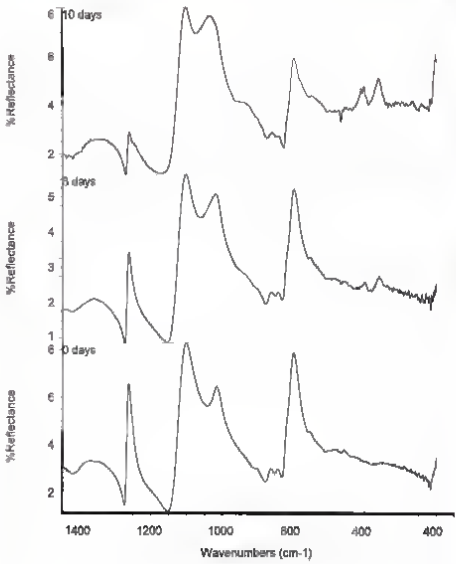

Figure 4-26: FTIR spectra of 70 Mesh samples reacted in SBF for 0, 3, and 10 days at 37°C

[illegible] 70 Mesh sample is reacted for 10 days in SBF, then [illegible] of crystalline P-O peaks become much larger and the [illegible] (tetragonal) peak at 818 cm^{-1} is reduced suggesting [illegible] most of the silicone is being covered by HCA.

To investigate the stages of HCA formation on these 70 [illegible] samples, 1 cm disks were made and reacted in SBF for 0, [illegible], 7, 12, and 24 hours at 37°C. Elemental analysis of the concentrations of Ca, P, and Si in these SBF reaction solutions was performed using ICP and plots are shown in Figure 4-27. The data represent the mean of 2 sample solutions and the error bars represent the standard deviation of that mean. It must be noted that these solutions were the first to be analyzed using ICP and the Ca standard deviations were quite large. Refinement of the ICP method, by increasing the element time to 1008 msec for the Ca measurement (from 800 msec), reduced this fluctuation in measurement. However, there was not enough solution left to rerun these samples. The P level starts at that of SBF, increases slightly through the 3 hour time period and then decreases to a level much lower than SBF starting at 7 hours. This decrease is indicative of the P being consumed as part of the formation and growth of HCA on the surface. Although the standard deviations are high for the Ca measurements, this same trend can also be observed.

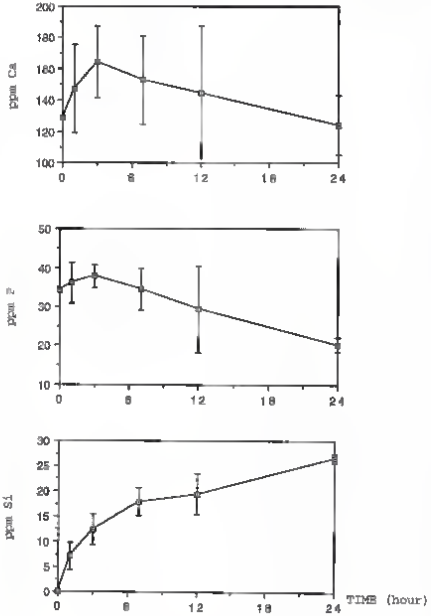

Figure 4-27: Plots of the elemental concentrations of Ca, P, and Si in SBF reacted with 70 Mesh samples for 1, 3, 7, 12 and 24 hours at 37°C

The level of Si in solution seen in Figure 4-3 [illegible]ts at 0 and increases over the entire reaction period to a final value of 26.6 ± 0.9 ppm.

4.5 Samples 70/45, 70/52, 70/55, & 70/60

To further investigate the reactions that occur between 3 and 12 hours, samples were made of bioactive glasses of various compositions using the same mesh technique, described above. The compositions and Ca/P ratio of the glass powders used are show in Table 4-1. These bioactive glass powders were obtained from U S Biomaterials and had the designations 45s5, 52s, 55s, and 60s.

Table 4-1: Bioactive glass compositions.

	SiO_2 (mole%)	Na_2O (mole%)	CaO (mole%)	P_2O_5 (mole%)	Ca/P ratio
45s5	46.1	24.4	26.9	2.6	5
52s	52.1	21.5	23.8	2.6	4.6
55s	55.1	20.1	22.2	2.6	4.3
60s	60.1	17.7	19.6	2.6	3.8

Disks were made of each of these and named 70/45, 70/52, 70/55, and 70/60. These disks were reacted in both Tris buffer and SBF for 3, 7, 9, 10, and 12 hours. FTIR analysis of their surface revealed no significant changes

and is [illegible] the strong reflection from the smooth silicone surface, as discussed above. SEM images of the surfaces reveal that HCA precipitation had occurred both on and between the glass particles after 12 hours in SBF with the 70/45, 70/52 and 70/55 samples. Figure 4-28, shows the typical growth of HCA around the glass particles on a 70/45 sample after 12 hours in SBF. Continuous layers of HCA could be observed for particles that were <25 μm apart, and a faint arc of growth is observed in the middle. In contrast, Figure 4-29 shows a 70/45 sample after 3 hours in SBF. No HCA growth was observed between the glass particles. Figures 4-30 and 4-31, show the typical growth on the surface of 70/52 samples after 12 hours in SBF. HCA growth was observed on and between the glass particles. Continuous growth was only seen when particles were <15 μm apart. Surrounding the large particle in the center of Figure 4-30, different amounts of HCA growth are seen; where particles are close continuous growth is seen and when distant spotty growth is observed. The typical surface of a 70/55 sample reacted for 12 hours is shown in Figure 4-32. Sparse HCA growth is seen between the glass particles on the surface. A 70/60 sample after 12 hours in SBF showed a total lack of HCA formation and the particle surfaces revealed silica gel formation (Figures 4-33 and 4-34).

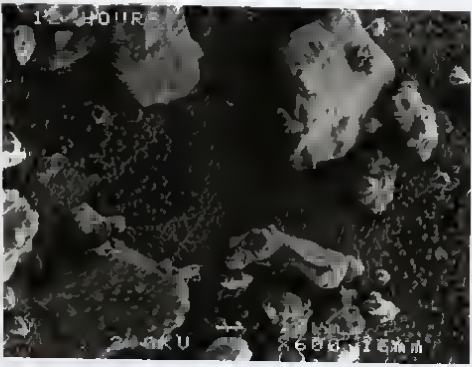

Figure 4-28: SEM micrograph of a 70/45 sample reacted in SBF for 12 hours at 37°C. HCA layer can be seen begining to form between particles.

Figure 4.9 SEM micrograph of a 70/45 sample reacted in SBF for 3 hours at 37°C No HCA growth can be seen between particles

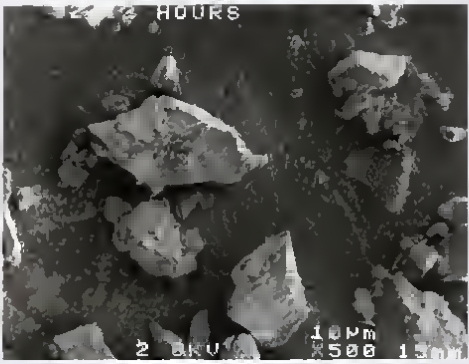

Figure 4-30 SEM micrograph of a 70/52 sample reacted in SBF for 12 hours at 37°C. HCA growth can be seen on and between the glass particles.

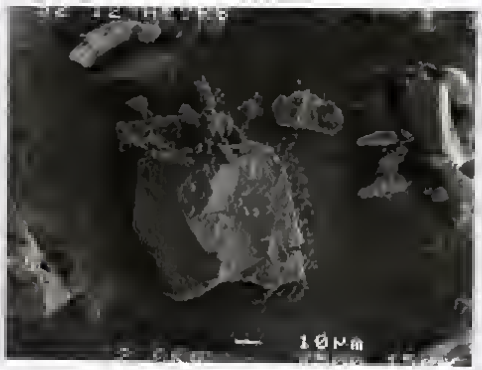

Figure 4-31 SEM micrograph of a 70/52 sample reacted in SBF for 12 hours at 37°C. HCA growth can be seen on and between the glass particles

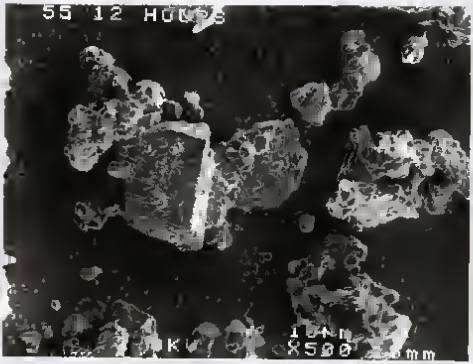

Figure 4-32 SEM micrograph of a 70/55 sample reacted in SBF for 12 hours at 37°C. Sparse HCA growth can be seen between the particles

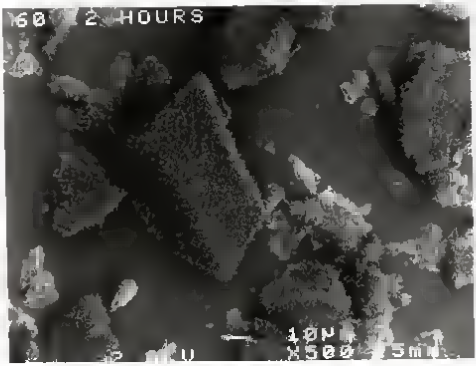

Figure 4-33 SEM micrograph of a 70/60 sample reacted in SBF for 12 hours at 37°C The particles reaction surface shows only silica gel

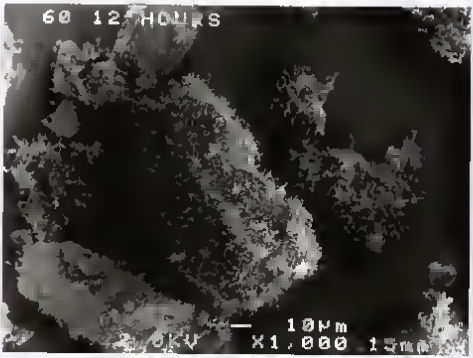

Figure 4-34 SEM micrograph of a 70/60 sample reacted in SBF for 12 hours at 37°C. The silica gel layer connects particles together

The square root of the distance between glass particles vs. the estimated percentage of silicone surface covered by HCA growth after 12 hours in SBF is plotted in Figure 4-35. These data were taken from the SEM micrographs shown in Figures 4-28 through 4-34. The distance was measured between solitary particles whose size ranged between 20 and 70 μm by using a ruler and the size bar located at the bottom right corner of the micrograph. Estimates of the percentage of HCA coverage were made by examining a 1 mm wide section centered on a line spanning the distance between particles. This section was further divided into 1 mm by 1 mm squares, the number of squares that had HCA particles was then divided by the total number of squares between the particles to get a percentage. This method was used due to the lack of contrast between the two surfaces and it was a simple estimate of the coverage. The maximum distance for 100% HCA coverage was greatest for the 70/45 glass and decrease with increasing SiO_2 content in the glass (i.e. 70/45 > 70/52 > 70/55). A linear curve fit is plotted along with each of these compositions and gave the best r^2 value (0.959, 0.991, and 0.986, respectively). Samples of 70/60 had no HCA formation on the glass particles themselves or on the silicone between them at any distance. The close linear correlation of a plot of HCA formation with the

square root of the distance suggests that this reaction is a diffusion controlled process. The concentration of drug release from polymers systems follows a similar relationship with release time and is shown in Equation 4-1 (Kli88).

$$M_t/M_\infty = k_1 t^{0.5} \qquad (4\text{-}1)$$

Where M_t/M_∞ is the concentration, t is the time, and k_1 is a diffusion constant. Time is proportional to the distance (d) by the velocity (v) of diffusion and therefore this equation is also proportional to the distance by Equation 4-2 (Wir97).

$$M_t/M_\infty = k_1 t^{0.5} \propto k_1 (vt)^{0.5} = k_1 d^{0.5} \qquad (4\text{-}2)$$

The diffusion control of the formation of HCA on silicone between bioactive glass particles further supports the theory that a zone of leached ions exists around these particles. The linear curve fits for all 3 glass compositions have similar decreasing slopes with distance suggesting that the HCA formation is similar in each case and that the concentration varies with distance. The only difference is how far apart the 100% coverage extends for each composition suggesting similar diffusion coefficients with an offset due to the initial glass concentration.

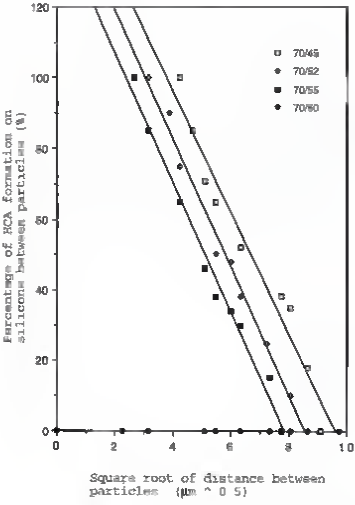

Figure 4-35 Plot of the square root of the distance between particles ($\mu m^{0.5}$) vs. the estimated percentage of HCA formation on the silicone between particles after 12 hours in SBF

Figures 4-36, 4-37 and 4-38 plot the elemental concentration of Ca, P, and Si (respectively) in SBF solutions as measured by ICP. Data points on each graph represent the mean of 3 reaction solutions (each with 3 measurements) for 70/45, 70/52, 70/55, 70/60 samples and uncoated silicone disks. The standard deviation of these means are represented as error bars on each data point. The lines connecting the points are drawn for clarification only. For the 70/45, 70/52, and 70/55 samples the Ca and P graphs have the same trend of an increase followed by a decrease in concentration as seen with the 70 Mesh samples in the previous section. The decrease is attributed to the precipitation and growth of HCA on the surface. Solutions from 70/60 samples had only small increases in the Ca and P levels but, no decrease after 12 hours reaction. The levels of Ca detected in solution increase in the same order as the amount of CaO present in the original glass composition (i.e. 45 > 52 > 55 > 60). This trend is not seen with the P levels since the amount of P_2O_5 in each glass composition is the same. The levels of Si detected in solution increase inversely with the amount of SiO_2 in each glass composition. Glasses with more SiO_2, have less Na_2O and CaO and are therefore more resistant to corrosion (Ada84 and Gro95). No elemental change was observed with the uncoated silicone

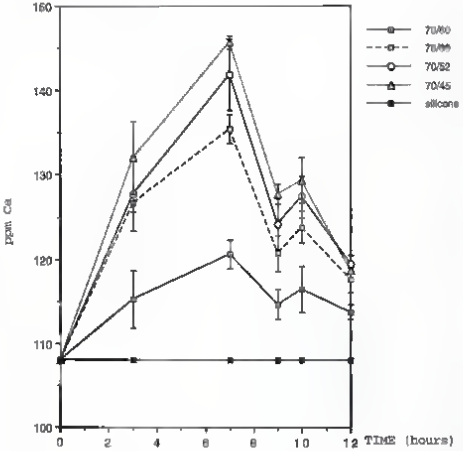

Figure 4-36. Plot of the elemental concentration of calcium in solutions of SBF reacted with 70/45, 70/52, 70/55, 70/60 and uncoated silicone disks for 0, 3, 7, 9, 10, and 12 hours at 37°C.

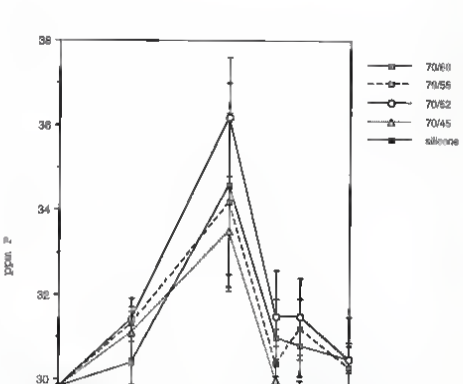

Figure 4-37 Plot of the elemental concentration of phosphorus in solutions of SEF reacted with 70/45, 70/52, 70/55, 70/60 and uncoated silicone disks for 0, 3, 7, 9, 10, and 12 hours at 37°C

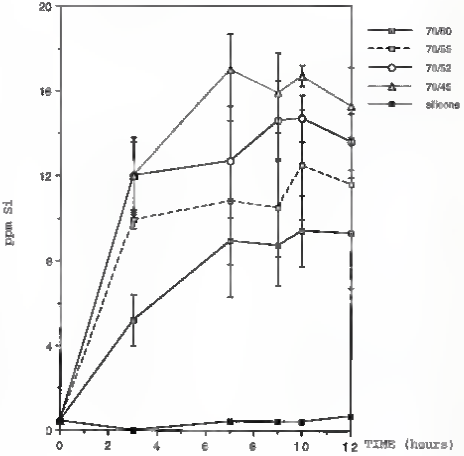

Figure 4-38 Plot of the elemental concentration of silicon in solutions of SOF reacted with 70/45, 70/52, 70/55, 70/60 and uncoated silicone disks for 0, 3, 7, 9, 10, and 12 hours at 37°C.

[redacted] of common ions such as Ca and P, on the leaching of these same glass compositions samples disks were also reacted in a Tris buffer devoid of Ca and P for the same time periods as above. Figures 4-39, 4-40 and 4-41 plot the elemental concentrations of Ca, P and Si (respectively) in Tris solutions as measured by ICP. Data points and error bars on each graph again represent the mean and standard deviation of 3 reaction solutions (each with 3 measurements) for samples of 70/45, 70/52, 70/55 and 70/60. Samples of 70/45, 70/52 and 70/55 all showed an increase in the amounts of Ca and P in solution with reaction time. In contrast, samples of 70/60 showed no increase in the Ca level and only a very small increase in the P level. The Ca level increases for 70/52 and 70/55 are in close agreement, increasing to ca. 6 ppm. Samples of 70/45 disks showed a larger increase in the Ca level (ca. 17 ppm). The increase in P levels for 70/45, 70/52 and 70/55 showed a very similar trend but, despite the fact that all 4 glass compositions had the same amount of P, samples from the 70/60 disks showed a much lower increase (>0.5 ppm). The trend observed with the Si levels in SBF was seen in the plot of the Si concentration in the Tris. The levels of Si detected in solution increased inversely to the amount of SiO_2 present in each glass composition.

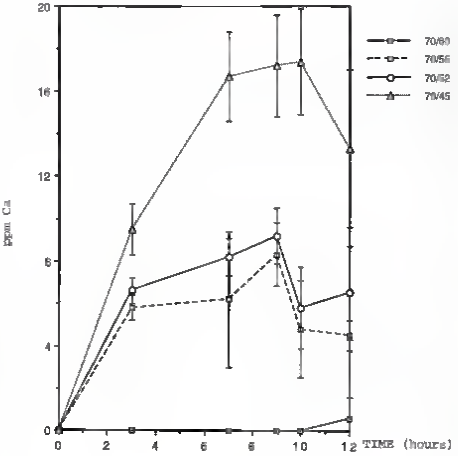

Figure 4-38 Plot of the elemental concentration of calcium in solutions of Tris reacted with 70/45, 70/52, 70/55 and 70/60 for 0, 3, 7, 9, 10 and 12 hours at 37°C.

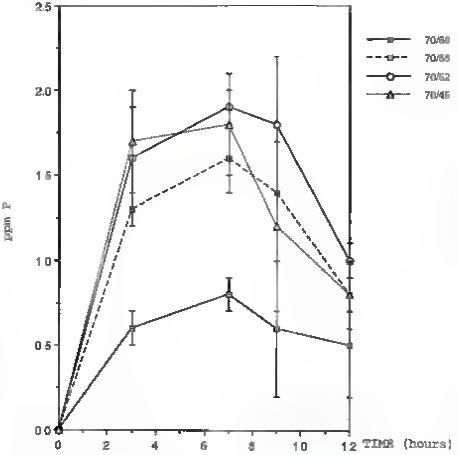

Figure 4-40 Plot of the elemental concentration of phosphorus in solutions of Tris reacted with 70/45, 70/52, 70/55 and 70/60 for 0, 3, 7, 9, 10 and 12 hours at 37°C

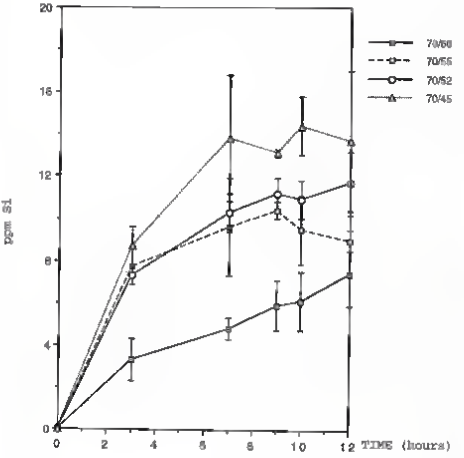

Figure 4-41: Plot of the elemental concentration of silicon in solutions of Tris reacted with 70/45, 70/52, 70/55 and 70/60 for 0, 3, 7, 9, 10 and 12 hours at 37°C.

Greenspan et al., examined the increase in surface area and average pore size with reaction time in Tris buffer for powders of these same glass compositions and found that 60s glass had little change in both after 7 days (Gre95). The authors described the bioactivity of these glass compositions as: bonding to bone and soft tissue with 45s and 52s; bonding to bone only with 55s, and no bonding with 60s. The study concluded that the large increase in surface area observed with both 45s and 52s was responsible for the rapid HCA formation (20 hours) and bonding to both tissues, while the moderate surface area increase seen with 55s induced slow HCA formation (3 days) and only bone bonding, the small increase in surface area of 60s glass was not sufficient to induce HCA precipitation even after 20 days in Tris (Gre95). This increase resistance to glass corrosion observed with the 60s glass may be the reason for the lack of P found in the Tris solutions, the absence of HCA formation on either the glass or silicone surfaces, and the presence of only a silica gel layer on the reacted glass surface after 12 hours reaction (Figures 4-33 and 4-34). Studies have shown that silica gel surfaces can induce the formation of HCA after 2 weeks reaction in SBF at 37°C or when implanted in the femurs of goats for 12 weeks (Li92a, Li92b, Li93, and Li95a).

The presence of a high surface area silica gel layer on the surface can induce HCA precipitation but, the presence of P in the glass influences the rate of HCA formation. The role of P, in a glass matrix, on the rate of HCA precipitation was studied by Ohtsuki et al. (Oht92). These authors found that a 50/50 $CaO-SiO_2$ glass would induce HCA to form in 3 days when reacted in SBF, in contrast the addition of 5 mole% P_2O_5 to this glass shorten this time to <12 hours in SBF (Oht92). Both a 50/50 $CaO-P_2O_5$ glass and a 50/5/45 $CaO-SiO_2-P_2O_5$ glass showed no HCA formation even after 7 days reaction in SBF. All 4 of the glass compositions were reacted in SBF, a solution that is saturated with respect to hydroxyapatite (Kok90a). ICP analysis by these authors showed that the reaction solutions showed a decrease in overall P level at the same time at the precipitation of HCA on the glass surface, solutions that did not induce HCA formation observed a steady increase in the P level through the duration of their reaction (Oht92). The formation of a silica gel layer on the glass surface induces HCA formation, but a localized increase in the P and Ca level catalyzes this formation.

A one-way analysis of variance (ANOVA) statistical comparison of the ICP data from both the SBF and Tris solutions was performed using InStat® (version 2.03,

GraphPad Software, San Diego, CA. Comparisons were made between the 4 glass compositions for each time period, element (Ca, P and Si) and solution. The results are presented in Table 4-2. In addition, a multiple pair-wise post test using a Student's t test was performed to compare each of the compositions, if the P value was >0.05.

Table 4-2: Results of ANOVA statistical comparison (P values >0.05 are **bold**)

SBF solution			
	Ca levels	P levels	Si levels
3 hours	P = 0.0023	**P = 0.1272**	P = 0.0008
7 hours	P = 0.0039	**P = 0.6756**	P = 0.0283
9 hours	P = 0.0004	**P = 0.2675**	P = 0.0071
10 hours	P = 0.0010	P = 0.0336	P = 0.0034
12 hours	P = 0.0009	P = 0.0312	P = 0.0328
Tris buffer solution			
3 hours	P < 0.0001	P = 0.0018	P < 0.0001
7 hours	P < 0.0001	P = 0.0008	P = 0.0035
9 hours	P < 0.0001	P = 0.0488	P < 0.0001
10 hours	P < 0.0001	**P = 0.8042**	P = 0.0005
12 hours	P = 0.0008	**P = 0.0739**	P = 0.0190

Variation among the compositions was significantly greater than expected by chance (P < 0.05) for all the time periods with the Ca and Si levels. The trends and differences observed with these 2 elements are statistically

significant throughout the reaction period studied. The variation among the compositions for the P levels is somewhat more complex, all the glasses have the same amount of P in them and should not be different. For the SBF solutions, statistically significant differences were observed with later reaction periods (i.e. after 9 hours). Review of the multiple pair-wise comparison shows that the differences observed after 9 hours are found between the 70/45 disks and the other sample disks, these differences are therefore due to the reduction in the P level caused by the formation and growth of the continuous HCA layer on the 70/45 disks. For the Tris solutions, the opposite is true, significant differences are seen at early reaction periods and not after 9 hours. The pair-wise post test revealed that the differences are observed between the 70/60 disks and the other samples. Early leaching of this corrosion resistant glass composition had very small P levels that were near the detection limit of P for ICP (0.2 ppm). The lack of resolution at these low levels could be responsible for the differences observed.

A statistical comparison of the increase in Ca, P and Si levels in SBF (above SBF base-line) and Tris was performed pair-wise for each element, time period and glass composition using a Welch unpaired approximate t test

There was no statistically significant difference found between the increase in SBF and Tris for elemental P or Si (average P = 0.3677 and 0.2334). A statistically significant difference was not observed between the increase in Ca levels of SBF vs Tris solutions (average P = 0.0644). Therefore common ions had little or no effect on the amount of Ca and P leached from the glass into the surrounding solution. These results are included in Appendix A.

4.6 Fine Bioactive Glass Powder

Recently, U.S. Biomaterials Corp., started manufacturing Bioglass® powder in a size range that had never before been made. This very fine size powder was made by using a "jet mill", a milling machine that uses very high pressure Argon gas to create a vortex inside a stainless steel container. Glass powder is introduced into this vortex and centrifugal forces cause the larger particles to move to the outer edge of the vortex, while the very smallest particles are allowed to reside in the center and exit the container. Particle-particle collisions at the outer edge of the vortex cause the glass particles to break apart. Once small enough, these particles exit through the center of the vortex. Size is controlled by the pressure of the gas creating the vortex and the number of times a powder

is passed through the vortex. The 45s5 Bioglass® particle size ranges obtained from U.S. Biomaterials were, <20 μm, <8 μm and <2 μm. Powders were spread on sheets of silicone that were coated with a thin layer of uncured silicone ("Y" samples) and uncoated silicone sheets ("N" samples). Preliminary tests had suggested that the uncured silicone might not be necessary for these fine sized particles. This was not the case. Disks made by coating with fine glass particles only and no uncured silicone showed a total dissolution of the particles and a haziness after 24 hours reaction in SBF but, FTIR analysis revealed no HCA on the surface of the disks. It is still unclear what reactions took place on the surface to produce the hazy appearance observed. Disks made with the thin layer of uncured silicone did produce a HCA coating on their surface and showed little dissolution of their particles (Figure 4-42). Figures 4-43, 4-44, and 4-45 show the reaction surface of disk of <20, <8 and <2 μm particles reacted for 24 hours in SBF. Shown are disk with the silicone layer (Y), disks without (N), and uncoated disks. Disks with the thin silicone layer show the formation of an HCA layer on their surface, represented as the P-O peaks at 600 cm^{-1}. Disks without the silicone layer and the uncoated disks do not.

Figure 4-42 Photograph of N<20 disk and Y<20 disk reacted in SBF for 24 hours at 37°C. With the uncured silicone Y sample the particles remain and without the particles are dissolved into solution

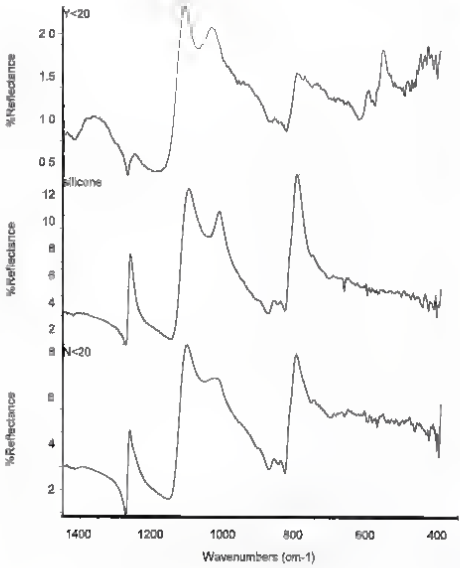

Figure 4.43 FTIR spectrum of disk with the silicone layer Y<20, uncoated silicone, and without the silicone layer N<20 reacted in SBF for 24 hours at 37°C.

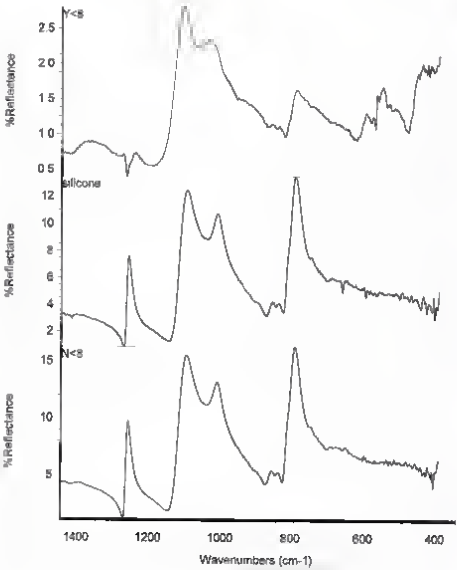

Figure 4-44: FTIR spectrum of disk with the silicone layer Y<s, uncoated silicone, and without the silicone layer N<s reacted in SBF for 24 hours at 37°C

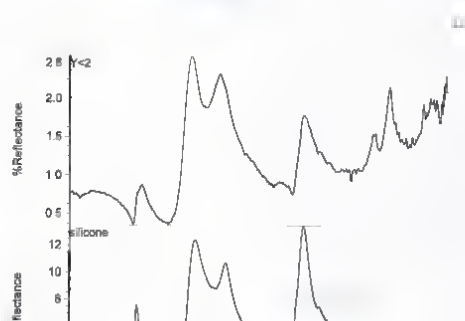

Figure 4-45: FTIR spectrum of disk with the silicone layer Y<2, uncoated silicone, and without the silicone layer N<2 reacted in SBF for 24 hours at 37°C

Fi[illegible] elemental concantrations of Ca, P and Si (r[illegible]tively) in SBF reaction solutions as measured by ICP. Data points on each graph represent the mean of 3 reaction solutions (each with 3 measurements). These graphs show that the Y samples (with the thin layer of silicone) have much higher Ca and Si levels than the N samples (without silicone layer). This result suggests that the Y samples may have more glass powder than the N samples and careful examination of the unreacted samples under light microscopy revealed that in fact the Y samples did have bi-layers and sometimes tri-layers of powder on the surface covering the thin silicone layer. Only a mono-layer of glass powder was observed on the N samples. Comparing the Y samples together shows close agreement and the same is true when the N samples are compared together. The formation of HCA on the Y sample surfaces can be related to the increase followed by decrease in both the Ca and P levels. Again the P levels drop to a level well below the original SBF level, suggesting that P is being used from the SBF to grow the HCA layer on the surface. No significant difference was measured between the different sizes of glass particles with respect to the levels of elemental Ca, P or Si in solution. This may be due the presence of similar size particles in all 3 samples

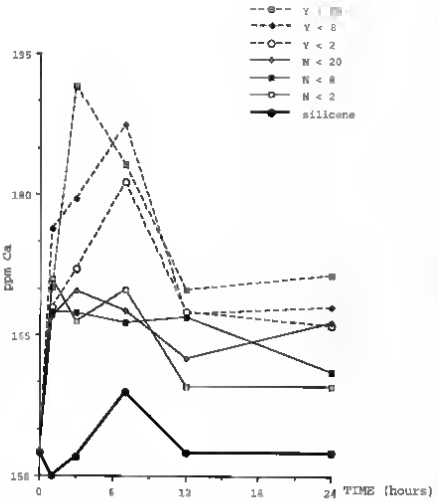

Figure 4-46 Plot of the elemental concentration of calcium in solutions of SBF reacted for 0, 1, 3, 7, 12 and 24 hours at 37°C

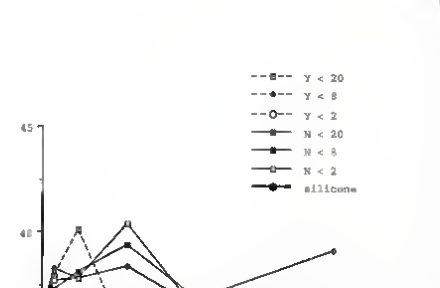

Figure 4 47: Plot of the elemental concentration of phosphorus in solutions of SBF reacted for 0, 1, 3, 7, 12 and 24 hours at 37°C.

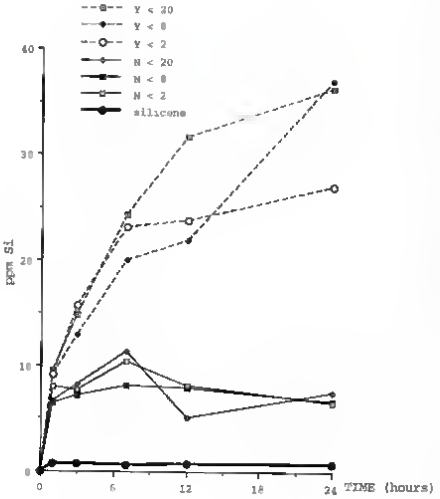

Figure 4-48: Plot of the elemental concentration of silicon in solutions of SRF reacted for 0, 1, 3, 7, 12 and 24 hours at 37°C.

4.7 pH Measurements

Throughout these experiments the pH of each solution was measured at 37°C after being reacted with the sample. Measurements were made at 37°C due to an observation that the increase in pH between room temperature (ca. 25°C) and 37°C was as high as 0.3.

In no case during this study did the pH of SBF or Tris buffer reacted with these samples increase more than the error of the pH probe (± 0.05). This result is in contrast to the results obtained by other researchers studying Bioglass® monolith samples *in vitro* (Hen71, Ogi80, Oht92, Kok92, Hen93a, Mei95 and Dem96). In all these other cases the ion exchange occurring at the glass surface was identified as the cause of the increase in solution pH. This ion exchange has been shown to produced silica-rich lesch layers at the glass surface reported to be as thick as 53 μm (Mei95). This reaction layer has been shown to become as thick as 300 μm *in vivo* (Wil93a). A gel layer that thick would be greater than the total size of the particles on the surface of our samples. Therefore, the lack of a pH increase in our studies is due to 2 related reasons: 1) the amount of buffer solution used is too large to observe a change in pH due to small amounts of ions being leached from

the particles and 2) the majority of ions leached from solution are used in the formation and growth of the HCA layer on the surface of these samples. The later reason is also supported by the reduction in the solution ion concentration of Ca and P.

4.2 Dip Coating of Catheters

Several combinations of soak time and silicone/hexane concentration were tested to produce the coated layer shown in Figure 4-49. Too much time or too high a concentration of silicone in the dipping solution resulted in a coated catheter with no bioactive glass exposed to the surface. Too little time or too low a concentration of silicone would result in an exposed glass coating that could easily be removed by gentle rubbing. Before coating excess solution was allowed to drip off the sample and the hexane was allowed to evaporate.

The resulting surface has bioactive glass particles imbedded in the final cured silicone surface. These glass particles can only be removed by scraping with a sharp blade, they will not rub off. The catheter material is still flexible, can be bent without particles flaking off and remains flexible even after 3 days in SBF at 37°C.

Figure 4-49: SEM micrograph of the cross-section of a broken catheter piece that has been coated with bioactive glass powder using a dip coating technique with 25% silicone/hexane

CHAPTER 5
CONCLUSION AND FUTURE WORK

5.1 Conclusions

This study has shown that the formation of hydroxycarbonate apatite (HCA) on the substrate surface between bioactive glass particles is a function of the particle size, composition and the distance between particles. The formation follows a diffusion controlled process with the rate proportional to the square root of the distance ($d^{0.5}$) between particles. The composition of the glass determines the off-set of this relationship. This conclusion can explain why composites made of only 10 to 20% bioactive glass show formation of HCA on the glass particles and not between them (Wen95). SEM micrographs revealed that the particles on these composites were indeed too far apart to form HCA between them.

In all cases the concentrations of Ca and P in solution decreased with the HCA formation on the surface. This represented a consumption of these ion for the formation and

growth of the apatite layer. This fact, coupled with the observation described above suggests a new theory that the formation of HCA on the surface was the result of a zone of leached ions present surrounding the glass particles. The concentration of this zone is dependant on the distance from the particles, and once a critical concentration is reached, formation of HCA occurs. The formation occurs first as an amorphous apatite layer and is converted into a crystalline HCA layer. This trend is similar to that observed for the formation of hydroxyapatite from saturated, moderately supersaturated and electrolyte solutions (Bre72, Fee79, and Bro91a).

This study was unable to observe a common ion effect on the total leached ions in solution. This may have been due to the localized nature of the formation of HCA on the surface and the limited effect that this formation had on the bulk solution. The limited effect was also observed in a lack of increase in the overall solution pH over the duration of this study.

This study has also shown that composites made of bioactive glass and silicone must have the glass exposed at the surface to be bioactive. This result is in contrast with a patent that describes a bulk mixed hydroxyapatite and silicone composite with excellent tissue adhesion (Fre96).

5.2 Future Work

First, the effect of bioactive glass coatings on peritoneal catheters needs to be examined in vivo. Long-term animal studies in either sheep or dogs seems to be the accepted model for this type of study. Special attention during implantation should be focused on the tightness of the seal at the exit-site, the rate of infection at the exit-site, and any extrusion of the catheter. Histological analysis after completion of the study would play a key role in determining the amount of epidermal downgrowth exhibited. Catheters both with and without Dacron cuffs still attached should be included in these experiments. The cuff may still be need to anchor the catheter in place for long-term stability.

Second, if this type of coating is successful then it need not be limited to peritoneal catheters. Hemodialysis catheters and other percutaneous access devices could make use of it. Power conduits for other implants may also benefit from a coating like this. In addition, drug delivery depots made of silicone implants could have improved release profiles. Currently, these devices form a fibrous capsule around them. This capsule is not well

vascularized and a barrier to drug release Implants that hava direct soft tissue adhesion may not hava this barrier to release and may improve the releasa profilas of the drug.

APPENDIX A
MEAN DATA

[illegible] 1-9, 4-10 and 4-11.

mean calcium in SBF (ppm) ± standard deviation (n=1)							
time	0.5 g	0.4 g	0.3 g	0.2 g	0.1 g	0.0g	SB
20 hour	95.5 ± 0.22	98.6 ± 0.44	94.6 ± 0.16	96.6 ± 0.52	153.0 ± 0.18	137.4 ± 0.94	129.8 ± 0.4o
6 hour	119.0 ± 0.49	113.0 ± 0.21	135.3 ± 0.88	137.7 ± 1.4	140.4 ± 0.31	134.2 ± 1.3	111 ± 1.1
2 hour	128.9 ± 0.51	123.6 + 0.39	147.1 ± 1.0	145.5 ± 0.49	136.1 ± 1.3	133.3 ± 0.76	110.1 ± 0.2
1 hour	150.3 ± 1.4	165.9 ± 3.4	154.4 ± 0.94	159.4 ± 0.71	142.9 + 1.1	136.9 + 1.7	166.0 ± 1.7
10 min	138.6 ± 0.47	140.3 ± 1.1	146.7 ± 1.3	149.1 ± 0.3	147.2 ± 0.26	142.8 ± 0.41	140.9 ± 1.4
0 hour	135.0 ± 2.2	135.0 ± 2.2	135.0 ± 2.2	135.0 ± 2.2	135.0 ± 2.2	135.0 ± 2.2	135.0 ± 2.2
mean phosphorus in SBF (ppm) ± standard deviation (n=3)							
20 hour	6.2 ± 0.04	4.4 ± 0.15	5.5 ± 0.13	5.0 ± 0.22	30.7 ± 0.09	31.4 ± 0.59	9.6 ± 0.16
6 hour	15.6 ± 0.24	13.4 ± 0.08	25.3 ± 0.93	31.1 ± 0.31	31.9 ± 0.4	31.3 ± 0.45	16.0 ± 0.15
2 hour	19.9 ± 0.45	22.6 ± 0.31	31.7 ± 0.3	31.5 ± 0.14	31.8 ± 0.47	31.3 ± 0.27	13.3 ± 0.13
1 hour	28.0 ± 0.17	33.2 ± 0.43	32.2 + 0.71	30.8 ± 0.28	30.3 ± 0.21	30.3 ± 0.44	32.2 ± 0.51
10 min	31.4 ± 0.09	31.7 ± 0.35	34.3 ± 0.77	35.9 ± 0.62	34.3 ± 0.23	33.5 ± 0.26	29.2 ± 0.68
0 hour	31.3 ± 0.1	31.3 ± 0.1	31.3 ± 0.1	31.3 ± 0.1	31.3 ± 0.1	31.3 ± 0.1	31.3 ± 0.1

mean elution in SAF (ppm) ± standard deviation (n=1)							
time	0.5 g	0.4 g	0.3 g	0.2 g	0.1 g	0.05 g	0.0 g
20 hour	33.5 ± 1.0	28.2 ± 0.62	26.9 ± 0.35	21.8 ± 0.16	19.9 ± 0.64	2.6 ± 0.0	42.9 ± 0.36
6 hour	15.4 ± 0.2	19.0 ± 0.51	15.2 ± 0.37	4.2 ± 0.06	5.6 ± 0.19	0.3 ± 0.04	14.4 ± 0.1
2 hour	12.3 ± 0.55	9.4 ± 0.57	9.7 ± 0.17	7.3 ± 0.0	2.0 ± 0.06	0.0 ± 0.02	18.5 ± 0.17
1 hour	13.8 ± 0.1	12.3 ± 0.16	6.9 ± 0.16	3.4 ± 0.12	1.1 ± 0.04	0.7 ± 0.2	11.7 ± 0.1
10 min	1.8 ± 0.07	2.2 ± 0.1	1.9 ± 0.0	1.2 ± 0.04	0.5 ± 0.1	0.3 ± 0.03	7.7 ± 0.04
0 hour	0.0	0.0	0.0	0.0	0.0	0.0	0.0

Data for Figure 4-19.

Mean concentration in SAF (ppm) ± standard deviation of 3 samples			
	ppm Ca	ppm F	ppm Si
0 day	131.8 ± 1.4	29.6 ± 0.6	0.7 ± 0.5
1 day	140.0 ± 9.7	21.1 ± 0.9	26.7 ± 5.2
5 days	134.2 ± 1.5	18.0 ± 0.6	38.5 ± 4.6
10 days	125.8 ± 1.6	17.3 ± 1.1	34.5 ± 4.2
20 days	123.3 ± 3.1	15.4 ± 2.5	37.7 ± 4.4

Data for Figure 4-27.

Mean concentration in SAF (ppm) ± standard deviation of 3 samples			
	ppm Ca	ppm F	ppm Si
1 hour	147.0 ± 28.3	36.1 ± 5.3	7.1 ± 2.7
3 hours	164.4 ± 23.3	37.8 ± 3.0	12.4 ± 3.0
7 hours	152.8 ± 28.3	34.5 ± 5.3	17.9 ± 2.7
12 hours	144.2 ± 42.9	29.4 ± 11.1	19.4 ± 4.0
24 hours	124.1 ± 19.2	20.2 ± 1.8	26.6 ± 0.9

Data for Figure 4-35

Estimated % HCA coverage as measured from SEM's after 12 hours					
distance (μm)	(μm^2 5)	70/45 (%)	70/52 (%)	70/55 (%)	70/60 (%)
0	0				0 0
5	2 236				0 0
7	2 646			100	
10	3 162		100	85	0 0
15	3 873		90		
18	4 243	100	75	65	
22	4 69	85			
26	5 099	71		46	0 0
30	5 477	65	50	38	0 0
36	6		48	34	
40	6 325	52	38	30	0 0
52	7 211		25		0 0
54	7 348			15	
60	7 746	38		0	0 0
65	8.062	35	10		
75	8 66	18	0		
83	9 11	0			
95	9 747				0.0

Data for Figures 4-36, 4-37, and 4-38.

mean calcium in SBF (ppm) ± standard deviation of 3 samples (normalized to silicone blank)					
	70/60	70/55	70/52	70/45	silicone
3 hours	115 2 ± 3 4	126 6 ± 1 0	127 7 ± 4 4	132 0 ± 4 3	108
7 hours	120 6 ± 1 7	135 4 ± 1 7	141 9 ± 4 2	145 7 ± 0 8	108
9 hours	114 6 ± 1 8	120 7 ± 2 2	124 1 ± 3 0	127 7 ± 1 2	108
10 hours	116 4 ± 2 8	123 8 ± 1 9	127 4 ± 2 4	129 3 ± 2 7	108
12 hours	113 7 ± 0 9	117 6 ± 1 6	119 4 ± 1 1	118 6 ± 0 4	108
mean phosphorus in SBF (ppm) ± standard deviation of 3 samples (normalized to silicone blank)					
3 hours	30 4 ± 0 5	31 3 ± 0 3	31 4 ± 0 5	31 1 ± 0 6	29 8
7 hours	34 6 ± 2 4	34 2 ± 2 1	36 2 ± 1 4	33 5 ± 1 0	29 8
9 hours	31 0 ± 0 9	30 4 ± 0 8	31 5 ± 1 1	30 8 ± 0 8	29 8
10 hours	30 8 ± 0 7	31 2 ± 0 7	31 5 ± 0 9	29 4 ± 0 6	29 8
12 hours	30 5 ± 0 3	30 3 ± 0 6	30 5 ± 1 0	28 8 ± 0 1	29 8
mean silicon in SBF (ppm) ± standard deviation of 3 samples					
3 hours	5 2 ± 1 2	9 9 ± 0 4	12 0 ± 1 8	12 0 ± 1 6	0 4
7 hours	8 9 ± 1 1	10 8 ± 4 5	12 7 ± 1 9	17 0 ± 1 7	0 4
9 hours	8 7 ± 1 9	10 5 ± 2 3	14 6 ± 1 9	15 9 ± 1 8	0 4
10 hours	9 4 ± 1 7	12 5 ± 2 6	14 7 ± 1 1	16 7 ± 0 5	0 4
12 hours	9 3 ± 2 6	11 6 ± 2 2	13 6 ± 1 3	15 3 ± 1 8	0 4

mean calcium in [illegible] (ppm) ± standard deviation of 3 samples

	70/60	70/55	70/52	70/45
3 hours	0 0 ± 0 1	5.8 ± 0 6	6.6 ± 0 6	9 5 ± 1 2
7 hours	0 0 ± 0 0	6 2 ± 3 2	8 2 ± 0 9	16 7 ± 2 1
9 hours	0 0 ± 0 0	8.3 ± 1 5	9.2 ± 1 3	17 2 ± 2 4
10 hours	0 0 ± 0 2	4.8 ± 2 3	5.8 ± 1 9	17 4 ± 2.5
12 hours	0 6 ± 1 0	4 5 ± 0 7	6 5 ± 2 2	13 3 ± 3 7

mean phosphorus in Tris buffer (ppm) ± standard deviation of 3 samples

	70/60	70/55	70/52	70/45
3 hours	0 6 ± 0 1	1.3 ± 0 1	1.6 ± 0 3	1 7 ± 0.3
7 hours	0 8 ± 0 1	1.6 ± 0 2	1.9 ± 0 1	1 8 ± 0 3
9 hours	0 6 ± 0 4	1 4 ± 0 4	1 8 ± 0 4	1 2 ± 0 5
12 hours	0 5 ± 0 3	0 8 ± 0 1	1 0 ± 0 1	0 8 ± 0 2

mean silicon in Tris buffer (ppm) ± standard deviation of 3 samples

	70/60	70/55	70/52	70/45
3 hours	3 3 ± 1 0	7 7 ± 0.0	7 3 ± 0 4	8 7 ± 0 9
7 hours	4 8 ± 0 5	9.6 ± 2 3	10 3 ± 0 9	13.8 ± 3 0
9 hours	5 9 ± 1 2	10 4 ± 0 4	11 2 ± 0 7	13 1 ± 0 2
10 hours	6 1 ± 1 4	9 5 ± 1 6	10 9 ± 0 9	14 4 ± 1 4
12 hours	7 4 ± 1 5	9.0 ± 0 5	11.7 ± 1 5	13 7 ± 3 3

Data for Figures 4-46 and 4-47.

mean calcium in SRF (ppm) ± standard deviation of 3 samples					
	1 hour	3 hours	7 hours	12 hours	24 hours
Y < 20	170 1 ± 6 2	181 6 ± 16 7	183 2 + 3 8	169 8 ± 23 4	171 4 ± 2 1
Y < 8	176 3 ± 4 8	179 5 ± 0 8	187 4 ± 3 2	167 3 ± 2 1	169 0 ± 7 5
Y < 2	168 0 ± 2 0	172 1 ± 2 0	181 3 ± 2 6	167 5 ± 5 6	166 0 ± 1 9
N < 20	167 0 ± 1 9	159 7 ± 12 7	167 6 ± 0 5	162 5 ± 0 2	166 3 ± 2 7
N < 8	167 5 ± 1 3	167 4 ± 2 0	166 3 ± 1 0	166 9 ± 2 5	161 1 ± 0 5
N < 2	171 0 ± 4 0	166 4 ± 1 1	169 8 ± 4 0	159 6 ± 2 1	159 6 ± 2 4
silicone	150 0 ± 5 2	152 0 ± 2 5	159 0 ± 5 0	152 5 ± 5 2	152 5 ± 5 2
mean phosphorus in SRF (ppm) ± standard deviation of 3 samples					
Y < 20	37 5 ± 1 8	40 1 ± 2 8	35 0 ± 0 6	29 7 ± 6 8	31 1 ± 1 3
Y < 8	36 0 ± 0 7	36 4 ± 0 1	35 0 ± 0 5	34 4 ± 1 0	27 0 ± 5 5
Y < 2	37 0 ± 0 6	36 5 ± 0 2	35 7 ± 1 3	33 6 ± 0 6	30 3 ± 1 7
N < 20	38 3 ± 0 0	37 8 ± 2 2	38 4 ± 0 1	36 7 ± 0 3	39 1 ± 0 5
N < 8	37 3 ± 0 1	38 1 ± 0 2	39 4 ± 0 2	37 2 ± 0 5	37 2 ± 0 5
N < 2	37 7 ± 0 3	37 8 ± 0 2	40 4 ± 0 8	36 8 ± 0 6	36 8 ± 0 5
silicone	36 5 ± 0 7	36 0 ± 2 0	36 0 ± 0 8	36 2 ± 1 8	36 0 ± 2 0

mean silicon in SBF (ppm) ± standard deviation of 3 samples					
Y < 20	9 6 ± 2 6	14 8 ± 1 5	24 3 ± 6 5	31 6 ± 10 7	36 ± 2 1
Y < 8	9 1 ± 1 4	12 9 ± 0-0	19 9 ± 2-5	21 8 ± 1 1	36 9 5-0
Y < 2	9 1 ± 1 1	15 6 ± 8-4	23 1 ± 2-3	23 7 ± 7 0	26 9 ± 5 2
N < 20	6 6 ± 0 6	8 2 ± 1 9	11 3 ± 1 2	5 0 ± 0 1	7 5 ± 3 5
N < 8	6 4 ± 0 3	7 1 ± 1 3	8 1 ± 0 4	7 9 ± 0 2	6 6 ± 0 3
N < 2	8 0 ± 0 8	7 7 ± 1 0	10 4 ± 1 0	8 1 ± 0 6	6 5 ± 1 4
silicone	0 8 ± 0 7	1-0 ± 0-7	1-0 ± 0-6	0 6 ± 0 7	1-4 ± 0 7

Data for common ion statistical analysis
Unpaired student's t test between 2 means
(two-tailed P values)
Are the increases in SBF values equal to Tris buffer values?

	3 hours	7 hours	9 hours	10 hours	12 hours
70/60 samples					
P	0.2315	0.1021	0.4020	0.3435	0.7040
Si	0.1258	0.0278	0.1198	0.0807	0.3530
Ca	0.0687	0.0411	0.0247	0.0359	0.0072
70/55 samples					
P	0.3876	0.1482	0.2615	0.2869	0.483
Si	0.0115	0.7208	0.9476	0.1973	0.1840
Ca	0.0003	0.0814	0.0645	0.0079	0.0369
70/52 samples					
P	1	0.0309	0.9959	0.1049	0.6566
Si	0.0477	0.1866	0.1007	0.0130	0.1959
Ca	0.0362	0.0092	0.0674	0.0046	0.0747
70/45 samples					
P	0.5196	0.5163	0.1637	0.1099	0.0051
Si	0.0527	0.2063	0.0530	0.1156	0.9324
Ca	0.0302	0.0583	0.1395	0.1637	0.3359

APPENDIX B
LIST OF PUBLICATIONS

1. Hench, LL, LaTorre, GP, Donovan, S, Marotta, J, Valliere, B, Properties of gel-silica optical matrixes with 4.5 nm and 9.0 nm pores. *Proc SPIE Int Soc Opt Eng* 1758: 94-104, 1992.

Abstract:

Sol-gel processing of tetra-Me orthosilicate with HNO_3 as a catalyst was used to make optically transparent silica matrixes with interconnected porosity of 1.2 to 1.4 nm radii. However, larger pores are often needed for impregnation of the matrixes with optically active orgs. Larger pore vols. are also desirable for many applications of these optical composites. Two methods for producing larger pore matrixes are compared. (1) catalysis with dil. HF; and (2) aging in a basic NH_4OH soln. Pore radii of matrixes made by the HF method are 5.0 nm after thermal stabilization at 900° and 4.4 nm after 1000°. Pore vols. are 0.9 cm/g at 900° and 0.7 cm^3/g at 1000°. The ammonia aging process yields 9.0 nm radius pores at 900° and 8.7 nm pores at 1000°. Optical properties (including UV cut-off, UV-vis-NIR transmission, IR absorption, index of refraction), bulk and structural densities of the matrixes made by both methods (900° and 1000° stabilization) are compared with the 1.4 nm pore radius matrixes.

2. Marotta, J, DePalma, D, Batich, C, Surface changes in 'silicone' elastomer upon exposure to saline. *Proceeding Society for Biomaterials Annual Meeting*, 14B, 1994.

Abstract:

Silicones have been used extensively in plastic and reconstructive surgery for the past 30 years. Their use has been in the form of elastomers, oils, and gels, with the most common silicone being poly(dimethylsiloxane) i.e. PDMS. Approximately 2 million women in the United States currently have silicone breast implants, comprised of gel and elastomer PDMS. PDMS has generally been assumed to be biologically inert because of its oxidative and thermal stability, and nonadhesiveness to tissue(1). This is due in part to the fact that PDMS is one of the most hydrophobic polymers known(2). Recently the biocompatibility of PDMS has come into question and its possible interactions with

the immune system are of great interest. It was noted that PDMS elastomer slowly becomes hydrophilic when exposed to saline for long times, and the following study examines this in more detail.

Sections of PDMS medical grade SILASTIC® sheeting (0.020" thickness) were cleaned in a sonicating bath of ultrapure water (NANOpure® system) for 30 minutes, rinsed twice and allowed to air dry. These samples were then extracted in toluene for 48 hours using a Soxhlet extractor to remove any low molar mass silicone.

Samples were then placed in a 0.9% saline solution at temperatures of 60°, 70°, 80°, and 100°C. A Pyrex® brand organic reaction vessel with a modified stir bar was used. Reactions were started with one PDMS sample and additional samples were added at subsequent times to make 1, 5, 10, 20, and 45 hour treatment samples. After 45 hours all samples were removed and rinsed twice with ultrapure water and allowed to set in a ultrapure water rinse bath for one hour. Samples were then analyzed using contact angle goniometer and X-ray photoelectron spectroscopy (XPS).

Prosil®221 (3-aminopropyltrimethoxysilane) was used to derivatize samples for analysis by XPS. XPS derivatization is an indirect measurement of the silanol concentration on the PDMS surface but is needed, since an oxygen atom bonded to a silicon atom would appear the same weather in the backbone or in a silanol configuration. As well, the vacuum needed for XPS could cause the silanol to reform into the backbone again. After treating samples in saline solution and rinsing with ultrapure water, they were place in a 5% solution of Prosil in ethyl alcohol and allowed to mix for 10 minutes. Samples were then rinsed with ethyl alcohol and cured in a desiccator for 24 hours a room temperature. High resolution XPS scans for C1S, O1S, S12P and N1S were made of the samples. The atomic concentration of nitrogen is assumed to be related to the concentration of silanol groups present on the PDMS surface.

Four control experiments were preformed to determine the effect of the reaction vessel on the changes of PDMS samples. The first control used a Pyrex® brand organic reaction vessel with the PDMS sample folded over and held by clamp rings. Saline solution was injected between the folds of PDMS and this setup was placed in the reaction vessel. The second control used a poly(methylpentene) 1-L PMP volumetric flask, the third used the PMP flask and 10 grams of PMP fragments in the flask, and the forth used the PMP flask and 10 grams of glass fragments in the flask.

Heating PDMS elastomer in a saline solution results in a hydrophilic surface (measured by contact angle goniometry). This is believed to be caused by the hydrolytic cleavage of the siloxane linkage (see Fig 1) Silanol groups are formed on the surface of the PDMS elastomer

This reaction follows an Arrhenius relationship The activation energy of the reaction can be derived from the slope of this Arrhenius plot This activation energy can then be used to calculate the time required to achieve a hydrophilic surface at body temperature, 37°C

The concentration of silanol groups on the surface of the PDMS was estimated using two techniques. contact angle goniometry and XPS derivatization Regression analysis of contact angle and XPS [%N] data was used to determine the silanol concentration on the surface. Controls of untreated PDMS were used as 0% silanol concentration Arrhenius plots of this data determined the activation energy required for the production of silanol groups on the surface of treated PDMS.

The activation energies calculated through these two methods were in close agreement, 4.6 Kcal/mol for the contact angle goniometry and 4 1 Kcal/mol for XPS derivatization. These values are in agreement with those found in the literature for a catalyzed thermal decomposition and a catalyzed stress-relaxation of PDMS(3-4) From the various control experiments, on the effects of the container used, it is believed that the surface silanol group concentration is due to the hydrolytic degradation of the PDMS and not the deposition of glass on the PDMS surface.

From the activation energy determined in this study, the time dependency for the formation of silanol groups on the surface of PDMS at body temperature can be calculated using the following equation

$$[SiOH] = k \ln(t) + [SiOH]_o \quad , \text{ where } k = k_o e^{(-E/RT)}$$

Because of the ln(time) function of the equation, a short initial exposure time produces a large change in the fractional surface coverage by silanol groups, from just over 12% for 12 hours to 20% in one month (making several assumptions about 'full' surface coverage)

It is clear that much additional work needs to be done to characterize the possible hydrolysis of PDMS in the body, before a complete understanding of this phenomenon is possible. These experiment were conducted using one type of highly filled PDMS The effect of this filler on the

hydrolysis of PDMS is currently being studied. These results, alternative explanations, and possible implications will also be discussed.

3. Yu, LT, LaTorre, GP, Marotta, J, Batich, C, Hardt, NS In vitro measurement of silicone bleed from breast implants *Plast Reconstr Surg* 97 756-764, 1995

Abstract

A method to measure gel bleed from intact silicone gel-filled breast implants was developed. This nondestructive technique permits accurate and reproducible serial measurement of silicone bleed from smooth wall breast implants (n=10) under simulated physiologic conditions in vitro. Gel bleed rates from new low bleed gel-filled implants and intact explants (unbarriered, low bleed, double lumen) were determined. These results demonstrate the reliability of this method to quantify silicone gel bleed and may permit a meaningful comparison of bleed rates from implants in the future.

4. Batich, C, DePalma, D, Marotta, J, LaTorre, G, Hardt, NS Silicone degradation reactions. *Curr Top Microbiol Immunol* 210 13-23, 1996

5. Wironen, J, Marotta, J, Bene, E, Batich, C. Surface properties of foley catheters relationship to bacteriuria and fouling. *Proceedings Fifth World Biomaterials Congress*, 175, 1996

Abstract

A variety of Foley catheters are currently available. Latex, 100% silicone elastomer, poly(vinyl chloride), hydrogel coated latex and silicone coated latex catheters are among the variety of products at the disposal of the medical industry. For several reasons, silicone elastomer coated (SEC) latex catheters are the most commonly used of these alternatives.

SEC catheters have been shown to possess the advantages of lower inflammatory response and lower kinetic friction. However, the rates of catheter-induced bacteriuria and encrustation are not significantly reduced when SEC catheters are used in lieu of standard latex catheters.

The goal of this study was to examine the interior and exterior surfaces of SEC catheters to determine their morphology and confirm or deny the presence of silicone.

A study relating surface morphology to the rates of bacteriuria and encrustation is currently underway.

SEC catheters, size 16 or 20 F, were obtained from the sales representatives for fourdifferent worldwide distributors of Foley cathaters. Two catheters from each of the four manufacturers were dried under vacuum for 24 hours. Dried catheters were frozen in liquid nitrogen and then broken in half. This method was chosen in preference to cutting with a blade since it is the belief of the authors that the latter technique may lead to artifactual delaminations of the silicone from the latex. Samples were selected at random and sputter coated with carbon using a Technique Hummer 5° sputter coater. SEM's were obtained of the interfacial region between the latex and the silicone of the luminal surface using a JOEL JSM 6400 scanning electron microscope. A second set of catheters (M-SEC) from one of the manufacturers was tested in a similar manner. The manufacturing process for these catheters had been modified to produce a smooth layer of silicone on the luminal surface.

SEM's were examined by 3 blinded judges. The judges studied the photos to determine whether there was silicone present, and if present, to measure the thickness of the layer.

No silicone was found on the luminal surfaces of two of the four brands of catheters. The silicone which was on the luminal surface of the other two brands was thin and did not present a smooth surface. The mean thickness of the silicone layer in these brands was 1 μm. The surface morphology observed in most brands was comprised of large scale holes (approximately 100um) with smaller cavities within. M-SEC catheters presented a thick (3 μm), smooth silicone layer on the luminal surface.

Axelsson and others have expressed the view that roughened surfaces may serve as nidi for the formation of fouling crystals. Additionally roughened surfaces may provide a better medium on which bacterial proliferation may occur. Considering that facultative anaerobes are the premier causative agent in bacteremia, the large scale holes and defects seen on the luminal surfaces may serve to provide favorable localized hypoxic areas in which these anaerobes may multiply.

Randalin, et al, and Kunin, et al, have not been able to show a significant difference between pure latex and silicone coated latex catheters when they studied their rates of encrustation. Additionally, other authors have obtained debatable results when they compared the rates of bacteriuria in SEC and latex catheters. It is likely that

the catheters used in these studies may not have had an adequate coating of silicone on their luminal surfaces. We submit that if the luminal surfaces of the catheters are adequately coated, that SEC catheters may behave in a manner similar to that seen with pure silicone catheters.

A microbiological study to confirm or deny these hypotheses is currently underway. The results of this additional study will also be presented. deny the presence of silicone. A study relating surface morphology to the rates of bacteriuria and encrustation is currently underway.

6 Marotta, J, LaTorre, GP, Batich, C, Hardt, NS, Yu, L: Measurement of silicon in tissue sites both adjacent to and distant from ruptured and intact silicone breast implants. *Proceedings Fifth World Biomaterials Congress*, 175, 1996.

Abstract:

The transport of silicone fluid to tissue sites distant from the tissue capsule, surrounding silicone breast implants, is a subject of great controversy. Emission techniques have been used to quantify the levels of elemental silicon (Si) in the capsules surrounding both intact and ruptured silicone breast implants.

The purpose of this study was to quantitatively measure the levels of silicon in tissues of rabbits with ruptured and intact silicone breast implants and infer from this the loading of silicone in these tissues.

Sixty rabbits were implanted with 3 groups of breast implants (125cc, Mentor, Corp.): 20 intact silicone gel-filled; 20 intact saline-filled; and 20 ruptured silicone gel-filled. Rabbits were implanted for periods between 3 months and 2 years. The following organs were removed for analysis: brain, capsule, heart, kidney, liver, lungs, pancreas, spleen, and regional nodes. Five unimplanted rabbits were used as controls. Sections of each organ were taken for pathological analysis. The remaining tissue was weighed, digested in 2 molar KOH, and the resulting solution was then analyzed with inductively coupled plasma (ICP) spectroscopy.

A total of 375 samples were analyzed to determine the concentration of elemental silicon (ppm Si or μg Si/ml). These concentrations were then converted to micrograms polydimethylsiloxane (PDMS)/gram tissue. Comparison of rates of occurrence of elevated PDMS levels (i.e. greater than control mean plus 2 standard deviations) among ruptured, intact and saline groups was performed (Fisher's exact test). Rates differed significantly among the 3

groups for brain tissue (P=0.031) and spleen tissue (P=0.042). A significant decreasing linear trend in rates from ruptured to intact to saline was noted for the brain tissue (P=0.035).

7 Marotta, J, LaTorre, GP, Natich, C, Hardt, NS, Yu, L: Measurement of gel bleed from silicone breast implants. *Proceedings Fifth World Biomaterials Congress*, 175, 1996.

Abstract:

Silicone gel consists of an insoluble crosslinked polymer and a mixture of lower molecular weight organic soluble components. The diffusion of these soluble components through the implant shell and into the surrounding tissue is known as "gel bleed". This group has developed a non-destructive technique that permits accurate and reproducible serial measurements of silicone "bleed" from intact breast implants under simulated physiologic conditions. A total of 28 explants, received from patients after removal, were tested *in vitro* at 2 week intervals for a period of 10 weeks.

The purpose of this study was to identify any significant differences in the bleed rates between types of explants.

A wide range of ages and manufacturers of breast implants were tested and include: unbarriered gel-filled (UNGF), low bleed gel-filled (LBGF) and double lumen gel/saline (DLGS) implants. Implants were immersed in a 1:1 implant volume to solution volume of simulated body fluid (SBF) that was maintained at 37°C for 2 weeks. At each 2 week interval Triton X-100 was added to the solution, the implant & solution sonicated for 20 minutes, the implant removed & rinsed with deionized water, and then the implant placed in a new jar containing fresh SBF. The concentration of elemental silicon (ppm Si) for each of these solutions was then measured using inductively coupled plasma (ICP) spectroscopy.

Silicone bleed levels for pairs of implants from the same patient were similar. No statistically significant trend was seen in the implant bleed rates vs. the age. Average values obtained were 11.9 ± 6.1 ppm Si/2 week for the UNGF, 14.9 ± 4.8 for the LBGF, and 20.6 ± 7.0 for the DLGS. The range observed was from 6.5 to 32.8 ppm Si/2 week. A slight statistical difference (P = 0.040) between the types of implants studied was observed.

8. Woronen, J, Marotta, J, Cohen, M, Batich, C
Materials used in urological devices. *Journal of Long-Term Effects of Implants* 7.1-28,1997

Abstract
The most commonly used materials in the manufacture of urological devices are discussed with respect to their application to urinary catheters, penile implants, testicular implants, artifical urinary sphincters, and urological stents. The manufacturing, physical properties, and general chemical and biological behavior of these materials are reviewed. Attention is paid to future research trends and the general conditions of the field of urological device materials

9. Goldberg, EP, Widenhouse, C, Marotta, J, Martin, F
Failure of silicone gel breast implants. Analysis of literature data for 1652 explanted prostheses. *Plast Reconstr Surg* 100 281-284, 1997.

10 Marotta, JS, Goldberg, EP Extraction studies with breast implant silicone elastomer shells and "gels" indicate very high concentrations of soluble uncross-linked silicones. *Proceeding Society for Biomaterials Annual Meeting*, 332, 1997

Abstract
So-called "gels" used in silicone gel-filled breast prostheses are not true gels in that these are actually compositions containing a minor amount of lightly cross-linked PDMS swollen with low molecular weight PDMS oil The properties of such "gels" are therefore greatly dependant upon their actual compostions. The soluble components of the PDMS elastomer shells are also important. Soxhlat extraction was performed on samples of elastomer shell and gel from silicone gel-filled breast implant controls and explants.

Migration of oil from the gel through the shell and into the body is referred to as "gel bleed" Estimates of the amount of soluble PDMS oils have ranged from 30% to 80% of the "gel" and the PDMS fluid is very soluble in the cross-linked silicone elastomer shell surrounding the gel.[1] In a sense, silicone gel-filled prostheses may be regarded as "controlled silicone release" implants and it is therefore important to know the composition of the "gels" and elastomers which have been so poorly identified to date

Silicone gel in this study was obtained from 3 unimplanted prostheses and 5 explanted pairs of silicone breast implants. Explant ages were 5, 6, 10, 15, and 19 years. Explanted specimens were sterilized with ethylene oxide prior to gel recovery. Specimens of elastomer shell were carefully dissected to obtain samples for other studies. Two samples of elastomer shell 2cm x 2cm were cut from each shell for extraction analysis. "Gels" were removed and stored at room temperature in clean polypropylene containers.

Elastomer samples were gently wiped with lint-free tissue to remove any superficial gel. Extraction of the "gels" involved adding 3-4 grams of weighed gel to a cellulose extraction thimble and then placing an additional thimble on top to create a sealed extraction thimble. This insured that no gel would float out during the extraction process. Extractions were performed using chloroform and were carried out until no further weight loss was detected in each sample (usually 3 days for the implant shell and 7 days for the implant gel). The values reported represent the soluble fluid portion of silicone in each of the samples. In the case of the shells, the soluble fraction includes fluid that has diffused or "bled" into the shell during storage and/or implantation.

Two gel samples and two shell samples from each implant were analyzed. The range of weight % extracted was: control shells 8.0-14.7%, explant shells 8.1-25.3%, control gels 86.6-91.2%, and explant gels 65.7-96.2%. The control shell extraction values are twice those previously reported by Ficha and Goldstein (5% weight loss of original unfilled shells, CUI, Inc.)[2]. Our values may be due to the fact that our control shells were stored gel-filled and soluble silicone from the gel diffused into them. The explant shell extraction values are twice the control values and could be a result of elastomer degradation and/or prolonged *in vivo* contact with gel for many years. The gel extraction values of all the implants, with the exception of the 19 year old explants, were much higher (84-96%) than previously reported. Gel extraction values for the 19 year old explants (66-68%) were lower than any other gel extraction values. This may result from the fact that early implants were filled with a more cohesive (more highly cross-linked) "gel". More recent implants were reportedly filled with gels that had extra silicone oil added by manufactures to give the "gels" a more "natural feel".

Implant gel extraction values are much higher than those suggested by the implant manufactures, as high as 96% uncross linked PDMS. This means that the amount of soluble silicone available for gel "bleed" is much greater than previously suggested.

A greater amount of soluble oil in the gel would mean that more oil is available to bleed from the implant while in the body.[3] Silicone oil that bleeds from implants can then be carried away by cells to other parts of the body.[4,5] The effect of this oil as a possible stimulus to immune problems is still under debate. But, swelling of the elastomer shell by the fluid component of the gel can result in a reduction of the elastomer tensile strength.[6] An FDA panel in 1992, commented that higher fluidity of implant gel implied "faster movement of liquid siliconas from within the gel mass to the shell and through the shell" and in the case of a ruptured implant "larger amount of chemicals could disburse from the exposed gel mass and dissipate throughout the body."[6] At that meeting, it was also noted that the lack of specifications for silicone gel manufacture would result in gels of variable consistencies and compositions. In this regard, our study affords new data concerning the compostions of silicone implant elastomers and "gels".

11. Widenhouse, CW, Marotta, JS, Kirk, JF, Amery, DF, Bhatia, S, Martin, F, Goldberg, EP. Comprehensive protocol for characterization of explanted silicone gel breast prostheses. *Proceeding Society for Biomaterials Annual Meeting*, 173, 1997.

Abstract.

Silicone gel breast implant safety remains controversial. As increasing numbers of implants are explanted, it is important to develop a sound data base to track the possible deterioration of properties that may lead to ruptures and other complications. A comprehensive physical and mechanical property test and evaluation protocol has therefore been developed for analysis of silicone gel breast implant controls and explants. Key aspects of the protocol and some preliminary data for 3 control and 10 explanted prostheses are presented here.

Visual and tactile appearance and integrity of the prostheses are observed and photographed prior to separating the gel from the shell. The elastomer shell is carefully cut into various samples for further analysis.

Mechanical properties are evaluated using tensile and tear testing, and dynamic mechanical spectroscopy (DMS). The tensile testing uses ASTM D 412-92; die D samples on a

model 1122 Instron with a strain rate of 20 in/min. The same instrument is used for ASTM type B tear testing (ASTM D 624-91). A Seiko 200 thermal analysis system is used for DMS analysis with sample dimensions of 6mm length and 9-12 mm width.

The gel flow (viscosity) properties are evaluated by a method we developed utilizing a Tinius Melt Flow Indexer Soxhlet extraction with chloroform is used to determine the soluble fraction of silicone within the gel and elastomer shell. Observations of the silicone shell surface morphology, integrity, topography and appearance are made using optical, low voltage scanning electron, and atomic force microscopy (OM, LVSEM, and AFM).

Sample integrity for explants ranged from intact samples with no visible shell defects, 4 of the 10 which were ruptured, one explant shell (5B-15 year) was completely obliterated, and some explants required very gentle handling to avoid tearing. The appearance, feel, and composition of the gel was variable, with some explants having very tacky and viscous gel, discoloration, and unidentifiable opaque inclusions. Some control samples contained foreign debris.

Tensile testing clearly identified a significant decrease in strength of the elastomer shell with time following implantation, for example, a decrease of 54-57% at 5 years. Tear strength of the explanted elastomers seemed strongly dependent on shell thickness and results will be reported when approximately 20 explants have been evaluated.

DMS analysis readily identified thermal transitions for the various elastomer materials. The T_g (-112 to 117°C), T_{melt} (-36 to -41°C), and a barrier layer Tg (-64 to -72 °C) where used.

Our newly developed Gel Flow Index (GFI) method used in this protocol provides reliable quantitative measurement of the gel flow properties at physiologic temperature, and appears clearly superior to previously used crude techniques [1]. The reproducibility of the method allows statistical comparison of sample data.

Soluble fractions removed from the gel by Soxhlet extraction in chloroform ranged from 65% (**2A**) to 96% (**5A**), and fractions removed from the elastomer shells ranged from 8% (**C-1**) to 27% (**2B**).

A high degree of variability was observed for these initial samples, and the comprehensive battery of physical, tactile, and mechanical analysis techniques is necessary for a through evaluation of explants. DMS is a useful additional tool for determining the dynamic modulus and thermal transitions, providing information on the composition and thermomechanical properties of the elastomer.

shell materials

The gel flow rheology has been characterized by a new method, GFI Analysis. Viscosity and flow properties of the gel can be reliably measured by this technique

Soluble fractions increase with implant time, and control values were found to be twice those reported previously by Ficha and Goldstain.[2]

The overall protocol, as demonstrated by initial test data, appears sound for characterization of silicone gel mammary prostheses implants and explants.

LIST OF REFERENCES

Abe90 Abe, Y., Kokubo, T., Yamamuro, T., Apatite Coating on Ceramics, Metals and Polymer Utilizing a Biological Process. J. Mater. Sci. Mater. Med. 1, 233-238, 1990.

Aba84 Adams, F.B., Glass Corrosion. J. Non-Crystl. Solids 67, 193-205, 1984.

And90 Andersson, O., The Bioactivity of Silicate Glass, Ph.D. Dissertation, Abo Akademi, Finland, 1990.

Abk87 Aoki, H., Akao, M., Shin, Y., Tsuzi, T., Togawa, T., Sintered Hydroxyapatite for a Percutaneous Device and Its Clinical Application. Med. Progress Tech. 12, 213-220, 1987.

Asa95 Asaoka, N., Best, S., Knowles, J.C., Bonfield, W., Characterization of Hydroxyapatite Precipitated from Different Reactants. In Bioceramics Volume 8, Wilson, J., Hench, L.L., Greenspan, D., Editors, Elsevier Science, Inc., New York, NY, 1995, 331-337.

Ash90 Ash, S.R., Chronic Peritoneal Dialysis Catheters: Effects of Catheter Design, Materials, and Location. Semin. Dial. 3, 39-46, 1990.

Ash94 Ash, S.R., Nichols, W.K., Placement, Repair, and Removal of Chronic Peritoneal Catheters. in The Textbook of Peritoneal Dialysis, Gokal, R., Nolph, K.D., Editors, Kluwer Academic Publishers, Boston, 315-334, 1994.

Bar94 Bard Access Systems VitaCuff® Antimicrobial Cuff Product literature, Bard Access Systems, Salt Lake City, UT, 1994.

Bre72 Brečević, L., Füradi-Muihofer, H., Precipitation of Calcium Phosphate from Electrolyte Solutions. Calc. Tiss. Res. 10, 82-90, 1972.

Brown76 Brown, W.E., Chow, L.C., Chemical Properties of Bone Minerals. Ann. Rev. Mater. Sci. 6, 213-236, 1976.

Bro91a Brown, P.W., Fulmer, M., Kinetics of Hydroxyapatite Formation at Low Temperature. J. Am. Ceram. Soc. 74, 934-940, 1991

Bro91b Brown, P.W., Hocker, N., Hoyle, S., Variations in Solution Chemistry During the Low-Temperature Formation of Hydroxyapatite. J. Am. Ceram. Soc. 74, 1848-1854, 1991

Cha95 Cheung, A.H.S., Wheeler, M.S., Limm, W.M.L., Wong, L.L., Fan, F.L., Wong, L.M.F., A Salvage Technique for Continuous Ambulatory Peritoneal Dialysis Catheters with Exit-site Infections. Am. J. Surg. 170, 60-61, 1995.

Cla76 Clark, A.E., Hench, L.L., Paschall, H.A., The Influence of Surface Chemistry on Implant Interface Histology: A Theoretical Basis for Implant Materials Selection. J. Biomed. Mater. Res. 10, 161-174, 1976

Cla90 Clark, A.E., Kim, C.Y., Wast, J., Wilson, J., Hench, L.L., Surface Reactions of Biologically Active Glass in Simulated Body Fluids. in Handbook of Bioactive Ceramics Vol. I, Yamamuro, T., Hench, L.L., and Wilson, J., Editors, CRC Press, Boca Raton, FL, 115-123, 1990

Coy96 Coyta, F.C., Young, L.G., Tippar, S.L., Mitchell, V.M., Stoffman, F.R., Williamsan, J., Geary, D.F., An Economic Evaluation of Hospital-Based Hemodialysis and Home-Based Peritoneal Dialysis for Pediatric Patients. Am. J. Kidney Dis. 27, 557-565, 1996

Dal88a Dalas, E., Kallitsis, J., Koutsoukos, P.G., The Crystallization of Calcium Carbonate on Polymeric Substrates. J. Cryst. Growth 89, 287-294, 1988

Dal88b Dalas, E., Kallitsis, J., Koutsoukos, P.G., Crystallization of Hydroxyapatite on Polymers. Langmuir 7, 1822-1826, 1991

Dalas, E , [illegible]tsis, J , Koutsoukos, P G , The Growth of Sparingly Soluble Salts on Polymeric Substrates Colloids and Sur. 53, 197-208, 1991

Daly83 Daly, B D T , Dasse, K A , Haudenschild, C C , Clay, W , Szycher, M , Ober, N S , Cleveland, R J , Percutaneous Energy Transmission Systems: Long-term Survival Tran. Amer. Soc. Artif. Int. Organs 29, 526-531, 1983.

Dea96 de Aza, P N., Guitian, F , Merlos, A , Lora-Tamayo, E., de Aza, S., Bioceramics-Simulated Body Fluid Interfaces pH and its Influence of Hydroxyapatite Formation J. Mater. Sci. Mater. Med. 7, 389-402, 1996.

Deg95 de Groot, K., Wolke, J.G.C., Bioceramics in Dentistry In Biocermaics Volume 8, Wilson, J , Hench, L.L , Greenspan, D., Editors, Elsevier Science, Inc , New York, NY, 1995, 275-278.

Dia95 Diaz-Buxo, J.A., Clinical Use of Peritoneal Dialysis In Nissenson, A.R., Fine, R.N , Gentile, D.E , Editors, Clinical Dialysis, 3rd Ed. Appleton & Lange, Norwalk, CT, 1995.

Dou67 Douglas, R.W., El-Shamy, T.M , Reactions of Glasses with Aqueous Solutions J. Amer. Cer. Soc. 50, 1-8, 1967.

Duc85 Ducheyne, P , Bioglass Coatings and Bioglass Composites as Implant Materials J. Biomed. Mater. Res. 19, 273-291,1985

Els96 Elsberg, L.L., Geometric Effects on Reaction Stages of Bioactive Glasses. Master's Thesis, University of Florida, 1996

Fee79 Feenstra, T.P., de Bruyn, P.L , Formation of Calcium Phosphates in Moderately Supersaturated Solutions. J. Phys. Chem. 83, 475-479, 1979

Fer94 Feriani, M., LaGreca, G., Kriger, F.L., Winchester, J.F., CAPD Systems and Solutions. In The Textbook of Peritoneal Dialysis, Gokal, R., Nolph, K.D., Editors, Kluwer Academic Publishers, Boston, 233-270, 1994.

Fuj84 Fujiu, T., Ogino, M., Difference of Bone Bonding Behavior Among Surface Active Glasses and Sintered Apatite. J. Biomed. Mater. Res. 18, 845-859, 1984.

Fur71 Füredi-Mulhofer, H., Purgarić, B., Srečević, L., Pavković, N., Precipitation of Calcium Phosphates from Electrolyte Solutions. Calc. Tiss. Res. 8, 142-153, 1971.

Gok93 Gokal, R., Ash, S.R., Helfrich, G.R., Holmes, C.J., Joffe, P., Nichols, W.K., Oreopoulos, D.G., Riella, M.C., Stingeneyer, A., Twardowski, Z.J., Vas, S.I., Peritoneal Catheters and Exit-Site Practices: Toward Optimum Peritoneal Access. Perit. Dial. Int. 13, 29-39, 1993.

Gok94 Gokal, R., Nolph, K., Historical Developments and Overview of Peritoneal Dialysis. In The Textbook of Peritoneal Dialysis, Gokal, R., Nolph, K.D., Editors, Kluwer Academic Publishers, Boston, 1-16, 1994.

Gre95 Greenspan, D.C., Zhong, J.P., LaTorre, G.P., The Evaluation of Surface Structures of Bioactive Glasses In Vitro. In Bioceramics Volume 8, Wilson, J., Hench, L.L., Greenspan, D., Editors, Elsevier Science, Inc., New York, NY, 1995, 477-481.

Gro84 Grosse-Siestrup, C., Affeld, K., Design Criteria for Percutaneous Devices. J. Biomed. Mater. Res. 18, 357-382, 1984.

Gro95 de Groot, K., Wolke, J.G.C., Bioceramics in Dentistry. In Bioceramics Volume 8, Wilson, J., Hench, L.L., Greenspan, D., Editors, Elsevier Science, Inc., New York, NY, 1995, 275-278.

Gup96 Gupta, S., Serardini, J., Piraino, S., Peritonitis Associated With Exit Site and Tunnel Infections. Am. J. Kidney Dis. 28, 415-419, 1996.

Hal75 Hall, C W , Adams, L.M., Ghidoni, J.J., Development of Skin Interfacing Cannula Tran. Amer. Soc. Artif. Int. Organs 21, 281-288, 1975

Hen71 Hench, L.L., Splinter, R.J , Allen, W.C., Greenlee, T.K , Bonding Mechanisms at the Interface of Ceramic Prosthetic Materials J. Biomed. Mater. Res. Symp. 2(1), 117-141, 1971

Hen80 Hench, L.L., Biomaterials Science 208, 826-831, 1980

Hen82 Hench, L.L., Ethridge, E.C , Biomaterials-An Interfacial Approach, Academic Press, New York, NY, 1982.

Hen84 Hench, L.L., Wilson, J., Surface-active Biomaterials Science 226, 630-636, 1984

Hen91 Hench, L.L., Bioceramics: From Concept to Clinic J. Am. Ceram. Soc. 74, 1487-510, 1991.

Hen93a Hench, L.L , Andersson, O., Bioactive Glasses In An Introduction to Bioceramics, Hench, L.L., Wilson, J., Editors World Scientific Publishing Co. Pte. Ltd., Singapore, 41-62, 1993

Hen93b Hench, L.L , Andersson, O., Bioactive Glass Coatings In An Introduction to Bioceramics, Hench, L.L., Wilson, J , Editors World Scientific Publishing Co Pte Ltd , Singapore, 239-259, 1993

Hol94 Holley, J.L., Bernardini, J , Perlmutter, J.A , Piraino, B., A Comparison of Infection Rates among Older and Younger Patients on Continuous Peritoneal Dialysis Perit. Dial. Int. 14, 66-69, 1994

Hua95 Huang, J., Wang, M., Rehman, I , Knowles, J., Monfield, W., Analysis of Surface Structures on Bioglass®/Polyethylene Composites In Vitro in Bioceramics Volume 8, Wilson, J , Hench, L.L , Greenspan, D , Editors, Elsevier Science, Inc , New York, NY, 1995, 389-395

Hum90 Hum, L., MacGregor, D., Mayar, D., Finchuk, L., Stokas, K., Tay, S., & Szychar, M., Letter to the Editor, J. Applied Biomater. 1, 193-194, 1990

Ito87 Ito, G., Matsuda, T., Inoue, N., Kamegai, T., A Histological Comparison of the Tissue Interface of Bioglass and Silica Glass. J. Biomed. Mater. Res. 21, 485-497, 1987.

Jan90a Jansen, J.A., van der Waerden, J.P.C.M., de Groot, K., Wound-Healing Phenomena Around Percutaneous Devices Implanted in Rabbits. J. Mater. Sci. Mater. Med. 1, 192-197, 1990

Jan90b Jansen, J.A., van der Waerden, J.P.C.M., van der Lubbe, H.B.M., de Groot, K., Tissue Response to Percutaneous Implants in Rabbits. J. Biomed. Mater. Res. 24, 295-307, 1990.

Jan91 Jansen, J.A., van der Waerden, J.P.C.M., de Groot, K., Development of a New Percutaneous Access Device for Implantation in Soft Tissues. J. Biomed. Mater. Res. 25, 1535-1545, 1991

Jan94 Jansen, J.A., Paquay, Y.G.C.J., van der Waerden, J.P.C.M., Tissue Reaction to Soft-Tissue Anchored Percutaneous Implants in Rabbits. J. Biomed. Mater. Res. 28, 1047-1054, 1994

Kan80 Kantrowitz, A., Freed, P.S., Clarkowski, A.A., Hayashi, I., Vaughan, F.L., VaShancey, J.I., Gray, R.H., Brabec, R.K., Barnstein, I.A., Development of a Percutaneous Access Device. Tran. Amer. Soc. Artif. Int. Organs 26, 444-449, 1980.

Kar89 Karlsson, K.H., Froberg, K., Ringbom, T., A Structural Approach to Bone Adhering of Bioactive Glasses. J. Non-Cryst. Solids 112, 69-72, 1989

Kea94 Keane, W.F., Vas, S.I., Peritonitis in The Textbook of Peritoneal Dialysis, Gokal, R., Nolph, K.D., Editors, Kluwer Academic Publishers, Boston, 473-502, 1994.

Kel59 Kelly, R.L., Vacuum Ultraviolet Emission Lines, Lawrence Radiation Lab, Menlo Park, CA, 1959

Kim89 Kim, C.Y., Clark, A.E., Hench, L.L., Early Stages of Calcium-Phosphate Layer Formation in Bioglasses, J. Non-Crystl. Solids 113, 195-202, 1989.

Kli88 Klier, J., Peppas, N.A., Solute and Penatrant Diffusion in Swellable Polymers VIII Influance on the Swelling Interface Number on Solute Concentration Profiles and Release J. Cont. Rel. 7, 61-68, 1988.

Kok90a Kokubo, T., Kushitani, H., Sakka, S., Kitsugi, T., Yamamuro, T., Solutions able to Reproduce In Vivo Surface-Structure Changes in Bioactive Glass-Ceramic A-W J. Biomed. Mater. Res. 24, 721-734, 1990.

Kok90b Kokubo, T., Surface Chemistry of Bioactive Glass-Ceramics J. Non-Crystl. Solids 120, 138-151, 1990.

Kok91 Kokubo, T., Yamamuro, T., Abe, Y., Process for Forming a Bioactive Hydroxyapaptite Film U.S. Patent 5,068,122, Nov 26, 1991

Kok92 Kokubo, T., Kushitani, H., Ohtsuki, C., Sakka, S., Yamamuro, T., Chemical Reaction of Bioactive Glass and Glass-Ceramics with a Simulated Body Fluid J. Mater. Sci. Mater. Med. 3, 79-83, 1992.

Kok93 Kokubo, T., Kushitani, H., Ohtsuki, C., Sakka, S., Yamamuro, T., Effects of ions dissolved from bioactive glass-ceramic on surface apatite formation J. Mater. Sci. Mater. Med. 4, 1-4, 1993

Kou81 Koutsoukos, P.G., Nancollas, G.H., Crystal Growth of Calcium Phosphates-Epitaxial Considerations. J. Cryst. Growth 53, 10 19, 1981

Kou87 Koutsoukos, P.G., Nancollas, G.H., The Mineralization of Collagen In Vitro, Colloids Sur. 28, 95-108, 1987

Kud90 Kudo, K., Miyasawa, M., Fujioka, Y., Kamegai, T., Nakano, H., Seino, Y., Ishikawa, F., Shioyama, T., Ishibashi, K., Clinical Application of Dental Implant with Root of Coated Bioglass: Short-Term Results. Oral Surg. Oral Med. Oral Pathol. 70, 18-23, 1990.

Lar95 Larmas, E., Sewon, L., Luostarinen, T., Kangasniemi, I., Yli-Urpo, A., Bioactive Glass in Periodontal Bone Defects: Initial Clinical Findings of Soft Tissue and Osseus Repair. in Bioceramics Volume 8, Wilson, J., Hench, L.L., Greenspan, D., Editors, Elsevier Science, Inc., New York, NY, 1995, 279-284.

LiP92a Li, P., Ohtsuki, C., Kokubo, T., Nakanishi, K., Soga, N., Apatite Formation Induced by Silica Gel in a Simulated Body Fluid. J. Am. Ceram. Soc. 75, 2094-2097, 1992.

LiP92b Li, P., Yang, Q., Zhang, F., Kokubo, T., The Effect of Residual Glassy Phase in a Bioactive Glass-Ceramic on the Formation of its Surface Apatite Layer *in vitro*. J. Mater. Sci. Mater. Med. 3, 452-456, 1992.

LiP93 Li, P., Ohtsuki, C., Kokubo, T., Nakanishi, K., Soga, N., Nakamura, T., Yamamuro, T., Process of Formation of Bone-like Apatite Layer on Silica Gel. J. Mater. Sci. Mater. Med. 4, 127-131, 1993.

LiP95a Li, P.J., Bakker, D., van Blitterswijk, C.A., A Hydroxyapatite-Polymer Composite Prepared by Mimicking Bone Mineralization. in Bioceramics Volume 8, Wilson, J., Hench, L.L., Greenspan, D., Editors, Elsevier Science, Inc., New York, NY, 1995, 435-439.

LiP95b Li, P., Ye, X., Kangasniemi, I., de Blaeck-Hogervorst, J.M.A., Klein, C.P.A.T., de Groot, K., In Vivo Calcium Phosphate Formation Induced by Sol-gel Prepared Silica. J. Biomed. Mater. Res. 29, 325-328, 1995.

LiR91a Li, R., Clark, A.E., Hench, L.L., An Investigation of Bioactive Glass Powders by Sol-Gel Processing. J. Applied Biomaterials 2, 231-239, 1991.

LiR91b Li, R., Sol-gel Processing of Bioactive Glass Powders. Ph.D. Dissertation, University of Florida, 1991.

Luz91 Luzar, M.A., Exit-Site Infection in Continuous Ambulatory Peritoneal Dialysis: A Review. Perit. Dial. Int. 11, 333-340, 1991.

Maj97 Majkowski, N.L., Mendley, S.E., Simultaneous Removal and Replacement of Infected Peritoneal Dialysis Catheters. Am. J. Kidney Dis. 29, 706-711, 1997.

Mar96 Marcologo, M., Ducheyene, P., Schepers, E., Garino, J., The 'Halo' Effect: Surface Reactions of a Bioactive Glass Fiber/Polymeric Composite In Vitro and In Vivo. Fifth World Biomaterials Congress 444, Toronto, Canada, 1996.

Mei95 Mei, J., Shelton, R.M., Marquis, P.M., Changes in the Elemental Composition of Bioglass During its Surface Development in the Presence or Absence of Proteins. J. Mater. Sci.: Mater. Med. 6, 703-707, 1995.

Monc94 Moncrief, J.W., Popovich, R.P., Dombros, N.V., Digenis, G.E., Oreopoulos, D.G., Continuous Ambulatory Peritoneal Dialysis. in The Textbook of Peritoneal Dialysis, Gokal, R., Nolph, K.D., Editors, Kluwer Academic Publishers, Boston, 357-395, 1994.

Neo92 Neo, M., Kotani, S., Nakamura, T., Yamamuro, T., Ohtsuki, C., Kokubo, T., Bando, Y., A Comparative Study of Ultrastructures of the Interfaces Between four kinds of Surface-active Ceramic and Bone. J. Biomed. Mater. Res. 26, 1419-1432, 1992.

Nie94 Niezgoda, J.A., Wolfson, A.B., Continuous Ambulatory Peritoneal Dialysis. Emer. Med. Clin. N. Am. 12, 759-769, 1994.

Chu91 Chura, K., Nakamura, T., Yamamuro, T., Kokubo, T., Ebisawa, Y., Kotoura, Y., Oka, M., Bone-bonding Ability of P_2O_5-Free CaO • SiO_2 Glasses. J. Biomed. Mater. Res. 25, 357-365, 1991

Oht92 Ohtsuki, C., Kokubo, T., Yamamuro, T., Mechanism of Apatite Formation on $CaO-SiO_2-P_2O_5$ Glasses in a Simulated Body Fluid. J. Non-Cryst. Solids 143, 84-92, 1992.

Ogi80 Ogino, M., Ohuchi, F., Hench, L.L., Compositional Dependence of the Formation of Calcium Phosphate Films on Bioglass. J. Biomed. Mater. Res. 14, 55-64, 1980.

Oka95 Okada, T., Ikada, Y., Surface Modification of Silicone for Percutaneous Implantation. J. Biomater. Sci. Polymer Edn. 7, 171-180, 1995.

Ore95 Oréfice, R.L., LaTorre, G.P., West, J.K., Hench, L.L., Processing and Characterization of Bioactive Polyaulfone-Bioglass® Composites. in Bioceramics Volume 8, Wilson, J., Hench, L.L., Greenspan, D., Editors, Elsevier Science, Inc., New York, NY, 1995, 409-414

Orr93 Orr, M.E., Issues in the Management of Percutaneous Central Venous Catheters. Single and Multiple lumens. Nurs. Clin. North Am. 28, 911-919, 1993.

Pre96 Prescott, A.D., Biocompatible Composite Material U.S. Patent 5,522,896, June 4, 1996

Paq96a Paquay, Y.C., de Ruijter, J.E., van der Waarden, J.P.C.M., Jansen, J.A., Tissue Reaction to Dacron® Velour and Titanium Fibre Mesh used for Anchorage of Percutaneous Devices. Biomaterials 17, 1251-1256, 1996.

Paq96b Paquay, Y.C., Jansen, J.A., Goris, R.J., Hoitsma, A.J., Long-term Clinical Experience with Continuous Ambulatory Peritoneal Dialysis: Access-related Problems. J. Invest. Surg. 9, 81-93, 1996.

San96 Santos, J D., Jha, L.J., Montairo, F J., In Vitro Calcium Phosphate Formation on SiO_2-Na_2O-CaO-P_2O_5 glass reinforced hydroxyapatite Composite: a Study by XPS Analysis. J. Mater. Sci. Mater. Med. 7, 181-185, 1996

She93 Sharartz, R J., Carruth, W A., Hampton, A A., Byron, M F., Solomon, D D., Efficacy of Antibiotic-coated Catheters in Preventing Subcutaneous Staphyiococcus aureus Infection in Rabbits. J. Infect. Dis. 167, 98-106, 1993.

Sio94 Sioshansi, P., New Process for Surface Treatment of Cathetars. Artif. Organs 18, 266-271, 1994

Smi85 Smith, H.O., DaVictoria, C L., Garfinkel, D., Anderson, P., Goldbarg, G L., Soeiro, R., Eiia, G., Runowicz, C D., A Prospective Randomized Comparison of an Attached Siiver-impregnated Cuff to Prevent Centrai Venous Catheter-associated Infection. Gynecol. Oncol. 58, 92-100, 1995.

Str71 Striker, G.E., Tanckhoff, H A M., A Tranecutaneous Prosthesis for Prolonged Access to the Peritoneal Cavity. Surgery 69, 70-74, 1971.

Squ81 Squier, C A., Collins, P., The Reistionship Between Soft Tissue Attachment, Epitheiial Downgrowth and Surface Porosity. J. Periodontal Res. 16, 434-440, 1981.

Suh94 Suh, H., Suh, S., Min, B., Anti-Infection Treatment of a Transcutaneous Device by a Coiiagan-Rifampicine Composite. ASAIO J. 40, M406-M411, 1994

Suh95 Suh, H., Wadhwa, N K., Cabralds, T., Subcutaneous Cuff Removei in Persistent Exit-Stie/Tunnei Infections in Peritoneal Diaiysis. Adv. Perit. Dial. 11, 157-159, 1995.

Suz95 Suzuki, K., Kagayama, Y., Toyoda, F., Nogimura, H., Harada, Y., Kokubo, T., Artifical Trachea made of Poymers Coated with Hydroxyapatite. in Bioceramics Volume 8, Wilson, J., Hanch, L.L., Greenspan, D., Editors, Eisavier Science, Inc., New York, NY, 1995, 351-356.

Tan95 Tan, M , Yao, T , Kokubo, T , Minode, M , Miyemoto, T , Nakamure, T , Yamamuro, T , Apetite Coeted on Orgenic Polymers by a Biomimetic Process Improvement in Adheeion to Substrate by Hcl Treetment J. Mater. Sci. Mater. Med. 6, 319-326, 1995.

Ten94 Tenaheshi, M , Yeo, T , Kokubo, T , Minoda, M , Miyemoto, T , Nekemura, T , Yamamuro, T , Apetite Coating on Orgenic Polymers by a Biomimetic Process J. Am. Ceram. Soc. 77, 2805-2808, 1994

TweEll Twerdowski, Z.J., Currently Used Cetheters-Adventages/Disedventages/Compications, end Catheter Tunnel Morphology in Humans. ASAIO J. 34, 937-940,1988.

Twa92 Twerdowski, Z.J., Perltoneal Dialyeie Catheter Exit Site Infectione: Prevention, Diegnosle, Treetment, and Future Directione. Sem. Dial. 5, 305-315, 1992.

Twe94 Twardoweki, Z.J , Khanna, R., Peritoneel Dielysis Access and Exit Site Cere in The Textbook of Peritoneal Dialysis, Gokal, R , Nolph, K D , Edltors, Kluwer Acedemic Publishers, Boston, 271-314, 1994.

USR96a U.S. Renel Data System: USRDS 1996 Annuel Data Report, Internationel Comperlson of ESRD Therapy Am. J. Kidney Dis. 28, S145-S151, 1996

USR96b U S Renal Deta System USRDS 1996 Annuel Date Report, The Economic Coet of ESRD and Medicere Spending for Alternetive Modelities of Treatment Am. J. Kidney Dis. 28, S127-S140, 1996

USR96c U S Renel Data System USRDS 1996 Annual Dete Report, Treetement Modalities for ESRD Petients. Am. J. Kidney Dis. 28, S48-S57, 1996.

Ves94 Vas, S.I , Infections Aeeociated with the Peritoneum end Hemodialyels In Bisno, A.L., Waldvogel, F.A., Edltors, Infections Associated with Indwelling Medical Devices, 2nd ed., Americen Society for Microbiology, Washington, DC, 1994, 309-346

von Recum, A F , Application and Failure Modes of Percutaneous Devices A Review. J. Biomed. Mater. Res. 18, 323-336, 1984.

Wan95 Wang, M., Bonfield, W., Hench, L L , Bioglass®/High Density Polyethylene Composite as a New Soft Tissue Bonding Material in Bioceramics Volume 8, Wilson, J., Hench, L L , Greenspan, D , Editors, Elsevier Science, Inc , New York, NY, 1995, 383-388.

Wil81 Wilson, J , Pigott, G H , Schoen, F J , Hench, L L , Toxicology and Biocompatibility of Bioglass J. Biomed. Mater. Res. 15, 805-817, 1981

Wil88 Wilson, J , Merwin, G E , Biomaterials for Facial Bone Augmentation Comparative Studies. J. Biomed. Mater. Res.: Applied Biomaterials 22(A2), 159-177, 1988

Wil90 Wilson, J , Nolletti, D , Bonding of Soft Tissue to Bioglass. In Handbook of Bioactive Ceramics Vol. I, Yamamuro, T., Hench, L L , and Wilson, J , Editors, CRC Press, Boca Raton, FL, 283-302, 1990

Wil93a Wilson, J , Clark, A E , Hall, M , Hench, L L , Tissue Response to Bioglass Endosseous Ridge Maintenance Implants. J. Oral Implantology 19, 295-302, 1993

Wil93b Wilson, J , Yli-Urpo, A , Happonen, R P , Bioactive Glasses: Clinical Applications In An Introduction to Bioceramics, Hench, L L , Wilson, J., Editors World Scientific Publishing Co Pte Ltd , Singapore, 63-73, 1993

Win74 Winter, G D , Transcutaneous Implants: Reactions of the Skin-Implant Interface. J. Biomed. Mater. Res. Symp. 5(1), 99-113, 1974

Wir97 Wirenen, J F., pH Controlled Drug Release for Dental Applications Ph.D. Dissertation, Univeraity of Florida, Gainesville, FL, 1997.

Yos91 Yoshiyama, N., Yoshizawa, K., Shin, Y., Aoki, H., Marumo, F., Bioactive Ceramics as Percutaneous Access Device (PAD) in Long-Term Peritoneal Dialysis. Perit. Dial. Int. 11(Suppl 1), 297, 1991.

Zab94 Zabetakis, P.M., Cotell, C.M., Chrisey, D.B., Auyeung, C.Y., Pulsed Laser Deposition of Thin Film Hydroxyapatite: Applications for Flexible Catheters. ASAIO J. 40, MB96-MB99, 1994.

Zab95 Zabetakis, P.M., Cotell, C.M., Chrisey, D.B., Medical Device with Infection Preventing Feature. U.S. Patent 5,385,295; Jan. 10, 1995.

Zho94 Zhong, J.P., LaTorre, G.P., Hench, L.L., The Kinetics of Bioactive Ceramics Part VII: Binding of Collagen to Hydroxyapatite and Bioactive Glass. In Bioceramics 7, Andersson, O.H., Yli-Urpo, A., Eds., Butterworth-Heinemann Ltd, 61-66, 1994.

BIOGRAPHICAL SKETCH

James Scott Marotta was born at Noble Army Hospital, Ft. McClellan, Anniston, Alabama, on May 27, 1968. Ft. McClellan has the distinct honor of being one of the few facilities in the world that still tests live nerve agent and biological weapons. His father was stationed there as a captain in the Army Chemical Corps, and his mother was a nurse at a local hospital.

In 1972, his family moved to Leesburg, Florida, where he lived until graduating from Tavares High School in 1986. After enlisting in the Florida Army National Guard, he was sent to Ft. Benning, Georgia, for Infantry Basic Training and Individual Advanced Training. During his 4 years of military service, he received 4 promotions, the Army Service Ribbon, several Company Certificates of Appreciation, an Army Certificate of Achievement, Florida Military Affairs-Certificate of Appreciation and the Reserve Overseas Ribbon for service in the Republic of Panama. During his National Guard service, he attended Lake Sumter Community College where he meet Dr. Edmund Cameron, a chemistry teacher that sparked his interest in chemistry.

After service in the National Guard, James moved to Gainesville, Florida, to attend the University of Florida. He was thrust into deciding a major after only 1 semester by the infamous "80 hour rule." He always enjoyed reading about exploration of space and space-craft so, he took a copy of his transcript to the aerospace undergraduate advisor and ask to be admitted to their program. At that time his only grade from the University was a C in Physics and admittance to the aerospace department was denied. He had to find a major or leave the University. Knowing that he wanted to pursue an engineering degree, he took his transcripts to each undergraduate advisor (in alphabetical order) and asked for admittance. Each one only looked at the sole University grade and denied him admittance except Dr. DeHoff of Materials Science and Engineering. He was admitted on a probationary agreement and that semester received 3 A's and 1 B+. One A was received in Numerical Methods a class taught by Dr. John Mahoney, the undergraduate advisor for industrial and systems engineering, who had said that James "did not belong in engineering."

After receiving his Bachelor of Science in Engineering from the University of Florida, James was admitted to the graduate program. In August of 1992, James began his

graduate studies under the supervision of Dr Christopher D Watch. While working in the area of biomaterials, he has performed a host of different projects involving several different medical devices from Foley catheter testing for an international medical device firm to the design of an *in vitro* bleed test and destructive testing of explanted breast implants.

I certify that I have read this study and that in my opinion it conforms to acceptable standards of scholarly presentation and is fully adequate, in scope and quality, as a dissertation for the degree of Doctor of Philosophy

Christopher D. Batich, Chairman
Professor of Materials
Science and Engineering

I certify that I have read this study and that in my opinion it conforms to acceptable standards of scholarly presentation and is fully adequate, in scope and quality, as a dissertation for the degree of Doctor of Philosophy

Anthony B. Brennan
Associate Professor of
Materials Science and
Engineering

I certify that I have read this study and that in my opinion it conforms to acceptable standards of scholarly presentation and is fully adequate, in scope and quality, as a dissertation for the degree of Doctor of Philosophy

Eugene P. Goldberg
Professor of Materials
Science and Engineering

I certify that I have read this study and that in my opinion it conforms to acceptable standards of scholarly presentation and is fully adequate, in scope and quality, as a dissertation for the degree of Doctor of Philosophy

Larry L. Hench
Graduate Research Professor
of Materials Science and
Engineering

I certify that I have read this study and that in my opinion it conforms to acceptable standards of scholarly presentation and is fully adequate, in scope and quality, as a dissertation for the degree of Doctor of Philosophy.

Karen A. Holbrook
Professor of Anatomy and Cell Biology

This dissertation was submitted to the Graduate Faculty of the College of Engineering and to the Graduate School and was accepted as partial fulfillment of the requirements for the degree of Doctor of Philosophy.

August, 1997

Winfred M. Phillips
Dean, College of Engineering

Karen A. Holbrook
Graduate School